Review Article

Norizan M. Nurazzi, Norli Abdullah*, Siti Z. N. Demon, Norhana A. Halim, Ahmad F. M. Azmi, Victor F. Knight, and Imran S. Mohamad

The frontiers of functionalized graphene-based nanocomposites as chemical sensors

https://doi.org/10.1515/ntrev-2021-0030
received February 17, 2021; accepted May 7, 2021

Abstract: Graphene is a single-atom-thick sheet of sp^2 hybridized carbon atoms that are packed in a hexagonal honeycomb crystalline structure. This promising structure has endowed graphene with advantages in electrical, thermal, and mechanical properties such as room-temperature quantum Hall effect, long-range ballistic transport with around 10 times higher electron mobility than in Si and thermal conductivity in the order of 5,000 W/mK, and high electron mobility at room temperature (250,000 cm^2/V s). Another promising characteristic of graphene is large surface area (2,630 m^2/g) which has emerged so far with its utilization as novel electronic devices especially for ultrasensitive chemical sensor and reinforcement for the structural component applications. The application of graphene is challenged by concerns of synthesis techniques, and the modifications involved to improve the usability of graphene have attracted extensive attention. Therefore, in this review, the research progress conducted in the previous decades with graphene and its derivatives for chemical detection and the novelty in performance enhancement of the chemical sensor towards the specific gases and their mechanism have been reviewed. The challenges faced by the current graphene-based sensors along with some of the probable solutions and their future improvements are also being included.

Keywords: graphene oxide, reduced graphene oxide, chemical sensor

1 Introduction

Graphene and its derivatives have been emerging materials for modern chemistry and physics owing to its fascinating properties profile since Andre Geim and Konstantin Novoselov (Nobel Prize winners for Physics in 2010) achieved groundbreaking experiments regarding the two-dimensional (2D) material graphene in 2004 [1]. Since its first isolation, the scientific development involving its synthesis methodologies and related applications has been inspiringly progressive, suggesting that graphene would revolutionize the industry with its superlative and promising properties [2,3]. Graphene has a high basal plane elastic modulus with 1 TPa, ultimate strength about 130 GPa, and room temperature charge carrier mobility by 10,000 cm^2/V s [3]. Graphene could be defined as a single layer of carbon atoms that are tightly packed to form a 2D honeycomb structure of sp^2 hybridized carbon [4]. Further extension of honeycomb network is the basic building block of other important allotropes, such as it can be stacked to form 3D graphite, rolled to form one-dimensional (1D) nanotubes, and wrapped to form 0D fullerenes [5]. The use of three π-electrons in carbon-carbon bonding results in a system of delocalized π-electrons perpendicular to the honeycomb plane giving rise to graphene's exceptional electrical properties.

Long-range of π-conjugation in graphene produces extraordinary thermal, mechanical, and electrical properties, which have long been the interest of many theoretical studies and more recently became an exciting area for wide range of applications [6,7]. In the applied field of research, among its wide range of applications, graphene has been largely used in batteries and cells as anodes and in supercapacitors due to its low charging time, high

* **Corresponding author: Norli Abdullah,** Centre for Defence Foundation Studies, Universiti Pertahanan Nasional Malaysia, Kem Perdana Sungai Besi, 57000 Kuala Lumpur, Malaysia, e-mail: norli.abdullah@upnm.edu.my
Norizan M. Nurazzi, Siti Z. N. Demon, Norhana A. Halim, Ahmad F. M. Azmi: Centre for Defence Foundation Studies, Universiti Pertahanan Nasional Malaysia, Kem Perdana Sungai Besi, 57000 Kuala Lumpur, Malaysia
Victor F. Knight: Research Centre for Chemical Defence, Universiti Pertahanan Nasional Malaysia, Kem Perdana Sungai Besi, 57000 Kuala Lumpur, Malaysia
Imran S. Mohamad: Faculty of Mechanical Engineering, Universiti Teknikal Malaysia Melaka, Hang Tuah Jaya, 76100 Durian Tunggal, Melaka, Malaysia

strength to weight ratio, and large surface area. Due to its unique properties which include a distinctive nanoporous structure, high mechanical strength, and high electrical and thermal conductivity, it has also found a large number of applications in areas like sensors, biomedical engineering, nano and flexible electronics, catalysis, and cement-based and geopolymer materials [8]. Besides that, a single atomic sheet of graphite has ignited intense research activities to clarify the electronic properties of this novel 2D electronic system [9]. However, charge transport in graphene is substantially different from that of conventional 2D electronic systems as a consequence of the linear energy dispersion relation near the charge neutrality point (Dirac point) in the electronic band gap structure [10,11]. This unique band gap structure is fundamentally responsible for the distinct electronic properties of carbon nanotubular graphene and carbon nanotubes (CNTs) [12].

Referring to Yavari and Koratkar (2012), the development of graphene-based chemical sensors presents the possibility of ultrahigh sensitivity detection of a range of gas species in air at room temperature and atmospheric pressure [13]. Before the beginning of graphene, there had been an extensive research on the starts of CNTs-based chemical sensors [14–16]. Graphene offers some important advantages compared to CNTs which is (1) a free-standing or suspended graphene sheet has both of its sides exposed to the chemical environment, thereby maximizing its sensitivity towards the analytes. Like multiwalled nanotubes, the inner cylinders are shielded from the chemical environment and even for single-walled nanotubes (SWCNTs), the ends may be closed (*e.g.* for tubes grown by chemical vapour deposition (CVD)), or the metal contact pads might cap the tubes and prevent the inside of the tube from participating in gas adsorption. (2) graphene exhibits inherently low electrical noise at room temperature [17], which arises from its unique 2D crystal lattice and high electron mobility. For these reasons, the sensitivity of graphene-based devices for molecular sensing is superior to that of CNTs. In truth, Schedin *et al.* (2007) have revealed that even the adsorption of single molecules could be detected using graphene [17].

This article provides a state-of-the-art review on performance of graphene's, graphene oxide (GO), and reduced graphene oxide (rGO) for chemical detection hybridized with metal oxide and conductive polymers have been reviewed. Their mechanism towards the specific gases also has been highlighted. The graphical abstract of the paper.

1.1 Graphene's characteristic

Cao *et al.* (2018) reported that arranging two layers of atom-thick graphene so that the pattern of their carbon atoms is offset by an angle of 1.1° makes the material a superconductor [18]. And although the system still needed to be cooled to 1.7° above absolute zero, the results suggest that it may conduct electricity much like known high-temperature superconductors [19]. Graphene already has impressive properties. It has shown superconductivity before, but it occurred when in contact with other materials, and the behaviour could be explained by conventional superconductivity [20]. Figure 1 shows a hexagon made up of two layers of graphene, twisted at an angle of 1.1°, had shown superconducting properties. Although graphene shows superconductivity at a very low temperature, it does so with just one-ten-thousandth of the electron density of conventional superconductors that gain the ability at the same temperature [21]. In conventional superconductors, the phenomenon is thought to arise when vibrations allow electrons to form pairs, which stabilize their path and allow them to flow without resistance. But with so few available electrons in graphene, it can somehow pair up which suggests that the interaction at play in this system should be much stronger than what happens in conventional superconductors like niobium-titanium alloy (type-II) with a superconducting critical material of 11 K [22].

In a global market, there are several types of graphene in a powder form material, such as GO, graphene nanoplatelets, graphene nanoribbons, and graphene quantum dots as well as graphene enabled products such as graphene ink or graphene masterbatches. Referring to Hernaez *et al.* (2017), the development of a method for the production of high-quality graphene in large quantities is essential to further exploit its full potential [23]. Hence, the use of GO and rGO has gained widespread consideration, as a compromise between the interesting properties of pristine graphene, the synthesization complexity, and cost. Figure 2 shows the schematic illustration of routes for preparation of GO and rGO from graphene flakes [24], whereas Table 1 shows the physical, mechanical, and electrical properties of the graphene materials [25–30].

GO can be synthesized by functionalizing with hydroxyl (–OH) or carboxyl (C═O) groups covalently bonded to a planar carbon network of graphite, *via* treatment with oxidizing agents such as sulphuric acid (H_2SO_4) and nitric acid (HNO_3). It is then exfoliated into few-layer or even monolayer GO, which nevertheless contains a high density of defects [31]. Small size of graphene

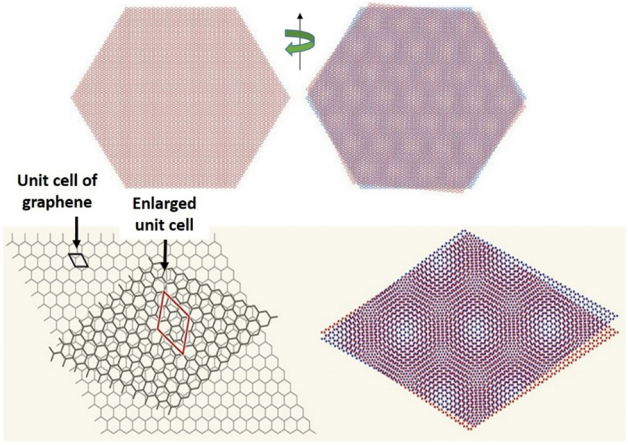

Figure 1: Two layers of graphene (right) that show a superconducting properties when it twisted at angle 1.1°. Adapted from ref. [21,22].

sheets can be obtained by subsequent reduction of GO, which can eliminate most of its oxygen-containing functional groups and partially recover its sp^2-bonded carbon network [32,33]. The abundance of functional groups in GO results in a hydrophilic behaviour which is strongly dependant on the level of oxidation. GO sheets show good dispersibility as a result of their strongly charged nature and hydrophilicity and form stable aqueous dispersions in a wide range of concentrations from 0.0125 to 0.05 wt% [34]. Additionally, GO are well-dispersed in organic solvents such as ethylene glycol, dimethylformamide, *n*-methyl-2-pyrrolidone (NMP), and tetrahydrofuran (THF) by forming hydrogen bonds between the surface and solvent interface.

1.2 rGO characteristic

In comparison to non-oxidized graphene nanoflakes, rGO is highly disordered with a relatively inferior quality due to the presence of many vacancy defects and Stone-Wales defects. Field emission electron microscope (FESEM) image presented at Figure 3 captured by Sharma *et al.* (2017) shows highly wrinkled and corrugated structure of rGO compared with GO, but shows liner (exhibit ohmic) *I–V* result for both GO and rGO. This outcomes present hint that both GO and rGO have the potential of being good gas sensing materials [35]. From FESEM in Figure 3(a) and (b), it is evident that surface of the sample gets corrugated upon reduction from GO to rGO due to reduction of oxygen-containing groups from the surface, while Figure 3(c) and (d) shows GO and rGO under high resolution transmission electron microscope (HRTEM) [36].

Furthermore, hydrogenated, fluorinated, and oxidized graphenes which are called fluorinated graphene or fluorographene are expected to have remarkable applications in coating, batteries, separation technologies, and electrochemical sensing. In another theoretical study, porous fluorinated graphene is suggested to modulate the heat of adsorption of molecules, enhancing the binding of dipolar ones (H_2O, SO_2, H_2S, and CO_2) over N_2, O_2, and CH_4 [37]. Therefore, applications are projected on separation of CO_2 and SO_2 from flue gases, purification of natural gas, and removal of H_2O from air. A significant benefit is expected for porous fluorinated graphene, related to the fact that gas molecule separation is not dependent on size-exclusion mechanism, but on interaction strengths.

The introduction of either acetylenic or diacetylenic chains between carbon hexagons is experimentally shown

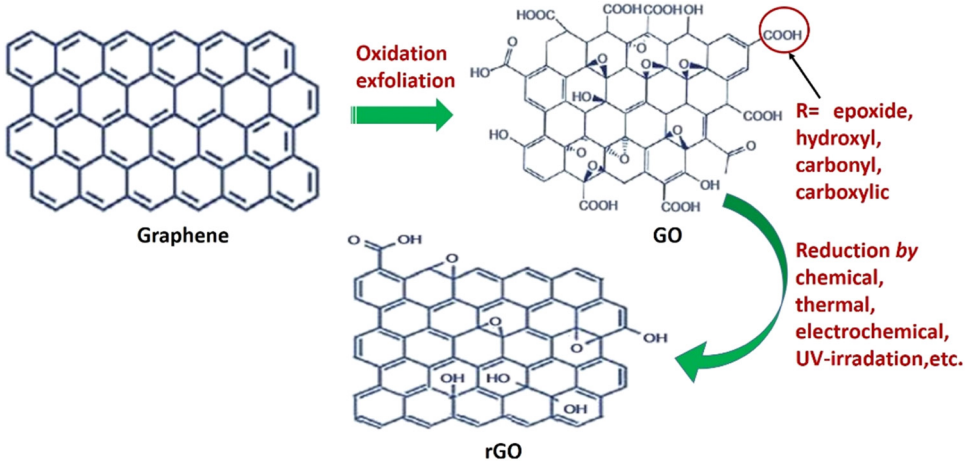

Figure 2: Schematic illustration of routes for preparation of GO and rGO. Adapted from ref. [24].

Table 1: Physical, mechanical, and electrical properties of graphene

Properties	Graphene	GO	rGO
Carbon (C), Oxygen (O) elemental ratio (%)	C (99)	C (62–65)	C (77–87)
	O (–)	O (35–48)	O (13–22)
Crystal size (nm)	175.49	21.14	15.13–15.95
d spacing (nm)	0.33	0.93	0.36
Plane size (μm)	0.5–5	1–2	1–7
Number of layers	3–5	1–3	1–3
Layer thickness (nm)	0.34	0.76–0.84	0.35–0.36
Stack thickness in water dispersion (nm)	180–230	1.00–1.20	125–175
Raman intensity ratio	0.25	0.79	1.10–1.16
Dispersibility in water	Not dispersible	Highly dispersible	Moderately dispersible
Tensile strength(GPa)	130	~0.13	—
Elastic modulus (GPa)	1,000	23–42	3.0–9.5
Elongation at break (%)	80	0.6	—
Electrical conductivity (S/m)	~1,000	Non conductive	~667

to give a layer of single-atom thickness, which is flat like graphene and is predicted to have interesting properties like graphene; the former is named graphyne and the latter graphdiyne [38]. Graphyne and graphdiyne cannot be prepared directly from graphene, but they are compared and discussed with graphene with respect to their structure and properties. Therefore, they are classified as graphene derivatives, together with graphane, fluorographene, and GO. Graphene-related nanomaterials, including doped graphene, graphene nanoribbons, and porous graphene, in addition to five nanomaterials, are classified as graphene derivatives. Figure 4 proposed by Inagaki and

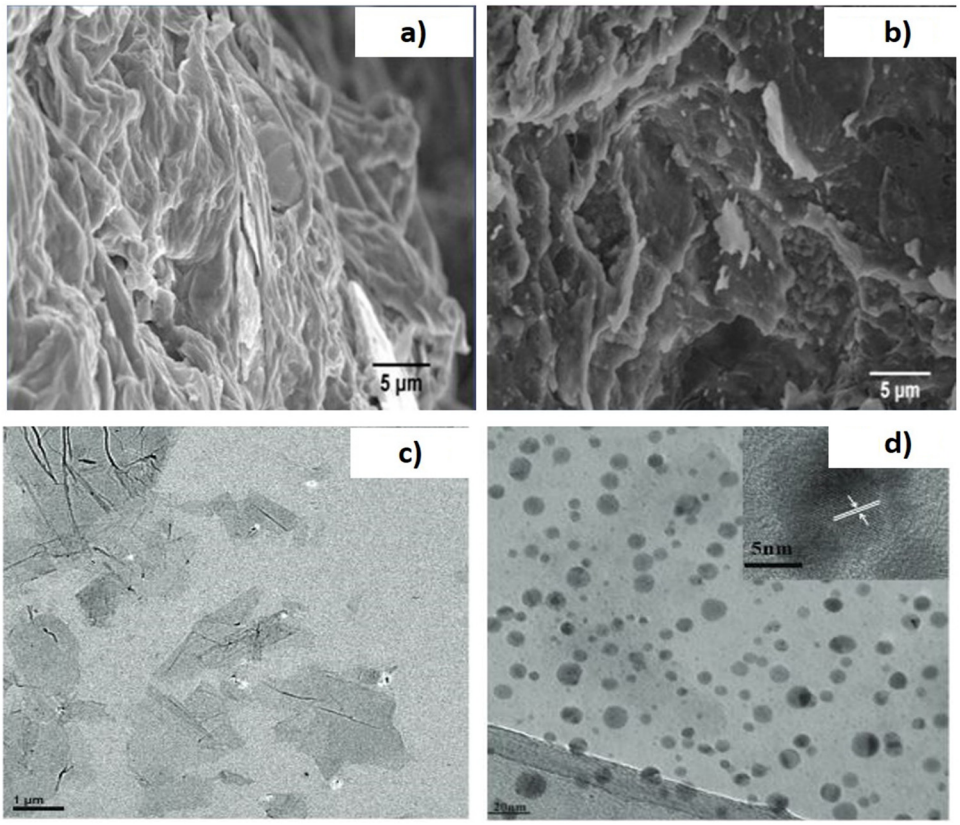

Figure 3: (a and b) FESEM images and (c and d) HRTEM image of GO and rGO–Au. Adapted from ref. [36].

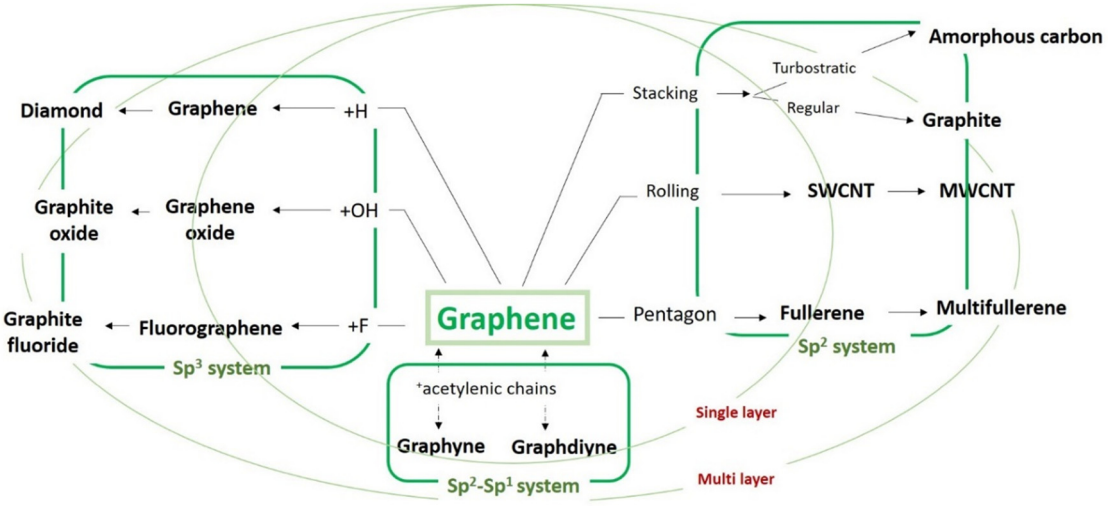

Figure 4: Schematic diagram of the development of graphene and its derivatives. Adapted from ref. [38].

Kang (2014) shows the development of graphyne and graphdiyne which suggests us a new carbon family composed of two kinds of C–C bonds, sp^2 and sp^1. However, graphane, fluorographene, and GO have to be included as new members of the sp^3 system. These carbon materials described in the present review can be derived by chemical reactions or theoretical considerations from graphene [38].

1.3 The discovery of graphenes as chemical sensors

These days, emissions of harmful by-products and pollutants, such as nitrogen oxides (NO_x), carbon oxides (CO_x), sulfur oxides (SO_x), and ammonia (NH_3), had increased significantly and endangered our health and environment over the long term. To monitor the chemical materials that are harmful to human health and the environment, chemical sensing devices have been extensively developed and explored. Improvement and optimization of present chemical sensors, including gas sensors as well as the development of new sensors that possess higher sensing performance with higher sensitivity but lower cost, are still necessary for not only industrial sectors but also indoor health and safety, environmental monitoring, and beyond.

The nanostructures of metal oxides like titanium oxide (TiO_2), Iron(III) oxide (Fe_2O_3), zinc oxide (ZnO), stannous oxide (SnO_2), tungsten oxide (WO_3), cuprous oxide (Cu_2O), *etc*. have been intensively explored for sensing applications. This is mainly due to their proven characteristics such as large specific surface area, excellent mechanical flexibility, good chemical stability, and better sensitivity [39–42]. However, metal oxide-based sensor materials hold certain limitations of high operating temperature (100–500°C), resulting in high power consumption, which in turn adversely affects the integration and long-term stability. In addition, metal oxide gas sensors are used since many decades to detect a gas species at high working temperature that is needed to promote gas reaction with the oxygen ionosorbed over the semiconductor, inducing a variation in the resistance of the material. As a matter of fact, high-temperature operation could raise the problem of ignition of fuels when detecting high explosive gases. Hydrogen, for example, can explode when mixed with atmospheric oxygen at concentration of 4% of lower explosive limit. Thus, room temperature detection is very important [43].

Besides that, common commercial gas sensors are based on semiconductor, polymer materials, and the methods used for sensing are optical methods, chemiresistive, calorimetric methods, gas chromatography, and acoustic methods, *etc*. [44]. The limitations of these gas sensors can be one or more of the following: costly, rare sensitivity in parts per billion (ppb), poor selectivity, limited life time, poor repeatability, difficult in miniaturization, and high power consumption [45,46].

As an alternative, nanomaterial-based gas sensing materials have gained significant momentum due to many promising electrical, optical, and thermal properties combined with high surface to volume ratio, short response and recovery times, high sensitivity, selectivity, reversibility, and stability [47,48]. Other than metal oxide, different

carbonaceous materials, such as CNT, charcoal, and carbon black, have been shown to be useful as chemical and biosensors due to the ease in tailoring their sensitivity through functionalization. Chatterjee *et al.* (2015) [49] had highlighted the other sides of graphene that can be considered the limitations. The problems related to intrinsic graphene are: (1) it is not producible in large scale, (2) it has no functional groups (required for gas/vapour adsorption), and (3) it has no band gap. The main performance enhancement techniques in graphene-based sensors are found to be doping [50], hybridization [51], functionalization [52], nano mesh formation [53], and field-effect transistor modulation [54]. In the context of rGO, a form of graphene, produced by reduction of GO which contains many functional groups and defects, has offered great potential as it is easy and cheap to produce in large scale. In addition, it can be easily functionalized, thereby generating and tuning the band gap energy. It is therefore no wonder that researchers have shown a great deal of interest in exploring rGO as a gas sensor candidate [55,56].

It was reported that the first graphene-based gas sensor was pioneering in 2007 by Schedin's and team [17]; demonstrated micrometre size sensors made from graphene are capable of detecting individual gas molecules that attach to or detach from the graphene surface. They showed that the adsorbed molecules change the local carrier concentration in graphene one electron by one electron, which leads to step-like changes in resistance. The achieved sensitivity is due to the fact that graphene is remarkably low-noise material electronically, which makes it a promising material not only for chemical detectors but also for other applications where local probes sensitive to external charge, magnetic field, or mechanical strain are required [17]. The gas-induced changes in resistivity had different magnitudes for different gases, and the sign of the change indicated whether the gas was an electron acceptor (*e.g.* NO, NO_2, O_3,) or an electron donor (*e.g.* CO, NH_3, C_2H_5OH). This research has created new possibilities for researchers to develop graphene-based gas sensors [57]. The interaction between graphene sheets and gas could vary from weak van der Waals to strong covalent bonding. All these interactions transform the electronic structure of graphene, which can be readily monitored by convenient electronic methods. Booth *et al.* (2008) and Hill (2011) indicated that the presence of interaction between target gas/vapour molecules could reach the lower limit of even a single molecule, *i.e.* high sensitivity even at low gas concentrations [58,59].

Recently, the use of graphene and its derivatives like GO, rGO, *etc.* [60–63] has been reported to show a promising sensing characteristic application due to its countless exceptional properties such as good thermal stability, ballistic conductivity, high carrier mobility at room temperature, low electrical noise due to its unique 2D honeycomb lattice as well as large surface area (theoretical surface area of 2,630 m^2/g) [17]. In addition, 2D materials can screen charge fluctuations better than 1D materials like CNT, *etc.* [64]. Referring to Ratinac *et al.* (2010), the most important reason graphene has been considered as a promising gas sensing material is that its electronic properties are strongly affected by the adsorption of gas molecules. Based on their discoveries, the planar structure of graphene eases Hall pattern fabrication and four probe measurements, limiting the contact resistance impact, and helps to focus only on the active area compared to its 1D counterpart, CNT [65,66].

Lu *et al.* (2011) reported that under a positive gate potential (n-type conductance), rGO exhibits sudden response and fast recovery for ammonia (NH_3) detection, far superior to the performance in p-mode at zero or negative gate potential [67]. In order to enhance the gas sensing performance of graphene, researchers have further explored chemical and physical functionalization of graphene with nanomaterials and in particular, conducting polymers, metals, and metal oxides such that a sizable energy gap can be opened up in graphene through the quantum confinement effect [68,69]. Russo *et al.* (2012) reported fabrication of room temperature hydrogen gas sensor from rGO, tin oxide (SnO_2), and platinum (Pt) with fast response and recovery times [70]. Paul *et al.* (2012) fabricated a sensor based on a nano mesh patterned from a CVD-grown large area graphene which exhibits sensitivities of about 4.32%/ppm of nitrogen dioxide (NO_2) and 0.71%/ppm of NH_3 with limits of detection of 15 and 160 ppb, respectively [71].

Furthermore, the involvement of graphene as GO and rGO in the developed sensors is attributed to some of the distinct advantages like the large surface-to-volume ratio, unique optical properties, excellent carrier mobility, and exceptional electrical and thermal properties compared to the other allotropes of carbon [72]. These properties are constant for the double and multilayered graphene structures. Apart from the difference in the structure and working conditions, the use of these advantages in graphene sensors lies mainly in their capability to adjust according to the application. For example, in strain sensors, properties like the detection limit, maximum sensing range, signal response, and reproducibility of the response hold a pivotal role to determine the quality of the sensor. These characteristics are attributed to the electrical and mechanical properties of graphene. In electrochemical sensors, its large surface area helps the loading of the desired biomolecules, resulting in the

interaction between the analyte molecule and electrode surface due to the high ballistic transport capability and the very small band gap. Another advantage of graphene materials is its low environmental impact, making it more popular for sensing purposes than other nanostructured metal oxides [49].

Chemical sensor is particularly interesting as it hybridizes the nanostructure of graphene with metal oxides to form hybrid nanostructures. This is because not only do they display the individual properties of the nanoparticles and of graphene, but may also exhibit additional synergistic properties that are desirable and advantageous for gas sensing applications; in other word, compliment the limitations on each for the desired detection and applications. One of the major advantages of such nanocomposite sensor is that graphene has near metallic conductivity with a possible inherent-amplified sensing configuration [49]. The high specific surface area of graphene may cause synergetic effects in achieving good gas response at room temperature when blended with metal oxides, especially on sensitivity and selectivity. Table 2 shows the structural and electrical properties of various types of carbonaceous materials.

While graphene and rGO exhibit ambipolar and almost symmetric behaviour in the electron and hole doping regions, they show p (hole)-dominant conducting properties because of the adsorbed water and oxygen molecules [73]. The strategy of hybridization of graphene with metal oxide will be discussed in the last part. To date, the unique optical, chemical, and morphological properties of graphene functionalized with conductive polymers, metal oxides, *etc.* are attracting a growing interest in the scholar's league. A closer look at Figure 5 in the number of publications reveals the rapid progress on the research of graphene and graphene composite-based gas sensors in the last decade. For the past ten years, about 886,000 number of publications related to the keyword "graphene" and about 41,700 number of publications related to the keyword "graphene chemical sensor" were found in Google Scholar (28th November 2020). In addition, about 25,500 number of publications related to "graphene composite chemical sensor" were found. These number indicate that graphene is becoming an interesting subject to be studied, and many more explorations can be done that could lead to huge impacts to the nation. This paper discussed the fundamentals of graphene and derivatives, the synthesization of graphene involved, the chemical modification of graphene involved, chemical sensor characteristics, and the performance of functionalized graphene for chemical sensor which includes hybrid of graphene with metal oxide and conductive polymers. This review ends with a conclusion and future perspectives of graphene materials in chemical sensors.

2 Chemical sensor characteristics and the basic mechanism

Chemical sensors are attracting tremendous interest because of the demand of sensitive, fast response, reversibility, and stable at low temperature sensor for public safety, space exploration, biomedicine, pharmaceuticals, for leakage detections of explosive gases such as hydrogen, for a real-time detection of toxic or carcinogenic gases in industries, and for the military purposes especially at the airport or at public area. Recently, extensive interest in improving reliable graphene-based chemical sensors has been rising as innumerable fields have been expanding. The key aspects expected for the development of a chemical sensor include sensitivity in the parts per million (ppm) to billion (ppb) range where the trace levels are involved, absolute discrimination, mild operation temperature, low power consumption, practical size, volume and mass, and low cost for large-scale applications [82,83]. Figure 6 explains a brief description of the four major important aspects for chemical sensor [84]. To satisfy these critical aspects and enhance the sensing performance, miscellaneous detection techniques for gas sensing have been explored and studied in the following section. This review begins with the sensing mechanism and working principles of the most prevalent gas sensing methods.

Sensor response traits of n-type and p-type gas sensors to different gases are summarized in Table 3 [85]. Because of these different characteristics, sensor response is defined according to resistivity of the active layer and in different ways depending on the type of measurements. Nevertheless, it is easily and commonly described as the ratio of resistance in air (R_a) to resistance in the presence of analyte (R_g) (R_a/R_g) for an n-type material with a reducing analyte. The response is expressed otherwise (R_g/R_a) for a n-type material with an oxidizing analyte [86,87]. It is *vice versa* for p-type sensors [88,89]. Although several compiled sensors make up a p–n heterojunction, they are decidedly sorted into their single dominant charge carrier trait of either n-type or p-type behaviour based on how resistivity decreases or increases in the augmentations of analyte concentration. This is to guarantee a straightforward understanding and an effective assessment of analyte sensing characteristics for both n-type and p-type gas sensors. The sensing response of p-type

Table 2: The structural and electrical properties of various carbonaceous materials including graphene

Carbon materials	Advantages	Limitations	Structural	Electrical	Reference
Amorphous porous carbon	High surface area, advanced porous system, abundant defective sites, superior chemical inertness	Relative low conductivity, poor adhesion with fluorine-doped tin oxide (FTO)	Consists of an outer spherical shell with porous interior structure A covalent random network composed of sp^3 and sp^2 hybridized carbons without grain boundaries Non-crystalline	High electronic conductivity and high surface area Electronic conductivity and ionic conductivity, with specific capacities of 212 mA h g^{-1} and 162 mA h g^{-1} at 0.5C and 1C, respectively.	[74]
Graphene	Excellent conductivity, fast charged carrier mobility, good mechanical strength, high optical transparency, good mechanical inertness, large surface area	Low surface area arising from the easy aggregation, low quantities of defective sites, high-quality thin film still lacking reproducibility, difficult to control bi-layer, tri-layer graphene, sheet resistance of tens or hundreds of nm thick layer is quite high	Crystalline carbon materials Monolayers of carbon atoms arranged in a honeycomb network Giant aromatic macromolecule	Conducts both electricity and heat Thermal conductivity and mechanical stiffness (3,000 W m^{-1} K^{-1} and 1,060 GPa, respectively)	[75]
Graphite	Good conductivity, corrosion resistance, excellent thermal stability	Poor porous system, low surface area	Stacks of graphene layers Weak interactions that hold the graphene sheets together	High electrical and thermal conductivity Thermal conductivity 25–470 W m^{-1} K^{-1} Electrical resistivity 5×10^{-4}–30×10^{-4} Ωcm	[76,77]
Carbon black	Plentiful defective sites, good chemical inertness	Low surface area, inappropriate pore size, inadequate conductivity	Typical particle sizes range from around 8–100 nm for furnace blacks	Highly structured carbon blacks provide higher viscosity Greater electrical conductivity and easier dispersion for specialty carbon blacks Electrical volume resistivity between 1 and 106 Ω cm	[78]
Carbon nanofibre	Excellent mechanical strength, high thermal conductivity, good chemical inertness	Insufficient conductivity, low surface area, inferior porous system	Cylindrical nanostructures with graphene layers arranged as stacked cones, cups, or plates Diameters from 50 to 200 nm	High electrical conductivity, and high thermal conductivity Intrinsic conductivity, at room temperature to be 5×10^{-5} Ωcm	[79,80]
Carbon nanotube	Large surface area, high electrical conductivity, good chemical inertness, shorter response and recovery times, reversibility and stability for raw CNT, ageing and thermal process increase the sensitivity of the sensors	Low quantities of defective sites, additional purifications and functionalizations required, lack of selectivity for raw CNT	Crystalline carbon materials Most of the physical properties of carbon nanotubes derived from graphene Carbon atoms are densely organized in a regular sp^2-bonded atomic-scale honeycomb (hexagonal) pattern	High electrical conductivity High thermal conductivity Resistivity of the SWCNT is 10^{-4} Ωcm at 27°C	[80,81]

Table 2: Continued

Carbon materials	Advantages	Limitations	Structural	Electrical	Reference
			sp^2 hybridization of carbon builds a layered construction with weak out-of-plane bonding of the van der Waals form and strong in-plane bounds	The SWCNT ropes able to sustain much higher stable current densities, as high as 10^{13} A/cm^2	

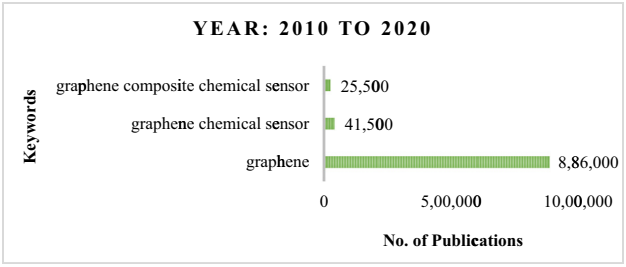

Figure 5: Progress of graphene-based chemical sensor in the last decade.

graphene-based chemical sensor over the chemical or analytes detection was determined using equation (1).

$$S(\%) = (R_g - R_o)/R_o \times 100 \quad (1)$$

Where R_o and R_g are the electrical resistance of graphene-based sensor before and after the exposure to analytes (*e.g.* NH_3) at specific time and temperatures, respectively.

Pristine graphene, GO and rGO, have presented a distinct gas sensing capability based on its structural characteristics. The 2D structure of graphene makes the electron transport through the graphene highly sensitive to the adsorption of gas molecules [90]. The adsorption of gas molecules on graphene's surface leads to changes in its electrical conductivity attributed to the change in the local carrier concentration. That change in the local carrier concentration is induced by the surface adsorbates which act as electron donors or acceptors [91]. All these materials have different electrical conductivity and surface functional groups, which play an important role in the gas sensing mechanism. For example, due to absence of functional groups in pristine graphene, the interaction occurs through the defects, and it possesses low intrinsic noise and high electrical conductivity even in absence of charge carriers; few charge carriers induced by the gas adsorbates lead to notable changes in charge carrier density resulting in detectable changes in electrical conductivity. In the following sections, we summarized the theoretical aspects of the sensing performance and related mechanisms on the detected gas of graphene-based materials followed by a detailed discussion on the state of the novel research work on applications of pristine graphene, GO, rGO, and functionalized graphene for gas sensing.

Referring to Jeevitha *et al.* (2019), the vapour sensing mechanism of rGO/metal oxide nanocomposites is governed by several factors like sensor porosity, specific surface area, and heterojunction formation. Metal oxide semiconductor-based sensors work on the principle of the change in resistance owing to the reaction among

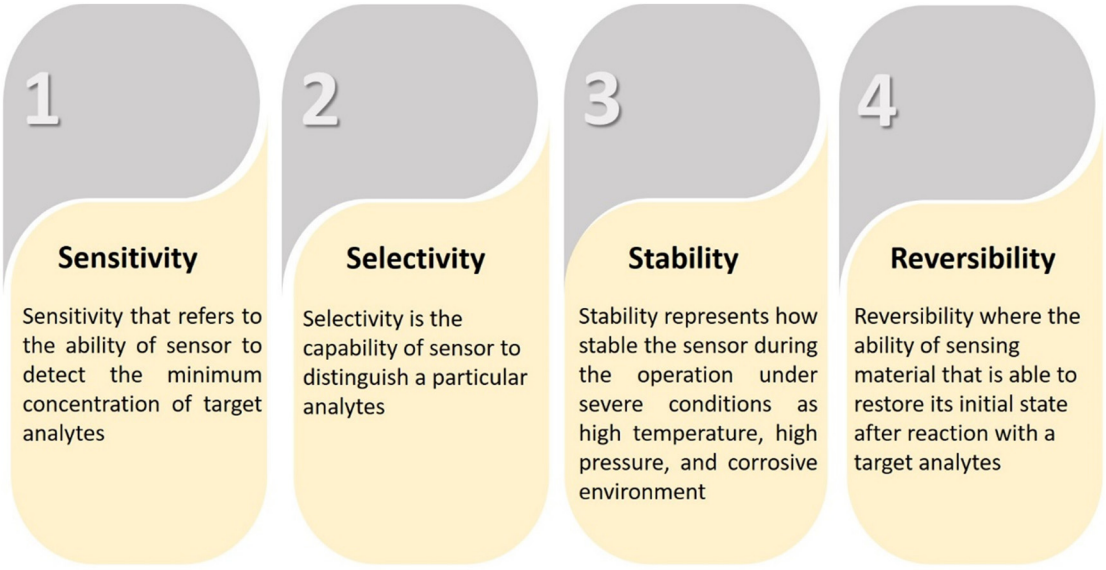

Figure 6: Four major important aspects for chemical sensor.

gas molecules and the sensitive surface. In the case of rGO/WO_3 nanocomposites, WO_3 is an n-type semiconductor and rGO behaves like p-type. It is well-known that the n and p type materials are dominated by electrons and holes, respectively. Once they come into contact with each other, a depletion layer is formed at the interface which is a p–n heterojunction. The rGO/WO_3 sensor shows p-type behaviour towards NH_3 detection. rGO possesses a higher work function and defects in the prepared nanocomposite surface, which will provide many adsorption centers for NH_3. Therefore, when the sensor surface is exposed to NH_3, the NH_3 molecules are adsorbed on the composite surface, and the interaction between adsorbed O_2^- and NH_3 releases free electrons and neutralizes the holes in the rGO which contributes to reduction in the width of charge conduction channels, leading to the increase in the width of the electron depletion layer, and hence an increase in sensor resistance [92].

The sensing behaviour of the polypyrrole (PPy)/rGO sensor is attributed to the electron transfer between NH_3 molecule and the rGO/PPy nanocomposite. As described at the equations (2) and (3), the PPy behaves like a p-type semiconductor. When the electron-donating NH_3 molecules adsorb onto the PPy surface, electrons transfer from NH_3 to the π backbone of the PPy [93]. This neutralizes holes in the PPy, thereby increasing the PPy resistance. For desorption of analytes, the electrons come back from the PPy to NH_3 and then the neutralized PPy becomes p-type, recovering the PPy resistance to its original value. The resistance changes from the electron transfer occurring on the surface of the PPy can be effectively transferred to the interdigitated electrodes (IDEs) through the rGO. It is worth noting that the electron transfers between the PPy and rGO is feasible due to the good interfacial affinity

$$\mathrm{PPy} + \mathrm{NH_3} \leftrightarrow \mathrm{PPy(NH_3\ adsorption)} \quad (2)$$

$$\mathrm{PPy,NH_3} \leftrightarrow \mathrm{PPy} + \mathrm{e(NH_3^+\ charge\ transfer)} \quad (3)$$

Besides that, the rGO includes a high density of sp^2-bonded carbons, vacancies, structural defects, and residual oxygen groups for a hole-transporting matrix, which behaves as a p-type semiconductor. The adsorbed NH_3 may transfer to the rGO matrix through the PPy layer and donating electrons to the rGO. The electrons transfer

Table 3: Sensing response behaviour of p-type and n-type sensors to reducing and oxidizing analytes

Sensing response behaviour	Examples of analytes	p-type sensor	n-type sensor
Reducing analytes	CO, NH_3, C_2H_5OH, SO_2	Resistance increases	Resistance decreases
Oxidizing analytes	NO_2, H_2O, F_2, Cl_2, Br_2, I_2, and O_2	Resistance decreases	Resistance increases
Dominant charge carrier	—	Holes (h^+)	Electrons (e^-)

depletes holes in the matrix, also increased the rGO resistance [94]. The synergistic effect of the PPy and rGO explains that the PPy/rGO sensor exhibits significantly higher sensitivity than the pristine rGO sensor. Although pristine PPy is a sensing material for NH_3 at room temperature, the response and recovery time is very long. The PPy layer allows electrons to quickly transfer between NH_3 molecules and the PPy/rGO nanocomposite. Besides, the presence of the PPy molecules on the surface of the rGO allows the complete interaction between NH_3 and the binding sites; the adsorbed NH_3 molecules can bind on the rGO through the PPy layer for the electron transfer. Therefore, the ultrathin PPy layer plays an important role in the PPy/rGO sensor response [95].

3 Performance of functionalized graphene in chemical sensor

3.1 Performance of graphene nanocomposite-based sensor

Graphene is highly sensitive towards changing chemical environment. This is because the suspended graphene has extremely high electron mobility at room temperature, and the electron transport in graphene remains increasing up to 0.3 μm at 300 K. Besides, in every carbon atom in graphene, there is a surface atom that provides the highest possible surface area per unit volume which leads the electron transport through the graphene and is highly sensitive to the adsorbed molecular species. The other factor is graphene has characteristically low electrical noise due to the quality of its crystal lattice and its high electron mobility [13]. These properties make graphene the best candidate for the ultrahigh sensitivity detection of different gases existing in various environments. High levels of sensitivity in detection processes are important for different industrial, environmental, public safety, and military applications [96].

The working principle for most of the graphene-based gas sensor is based on changes in their electrical conductivity due to the adsorption of gas molecules on the graphene's surface. These gas molecules act as donors or acceptors on graphene, similar to other solid-state sensors [97]. In 2007, Schedin and team were the first researchers team who fabricated a microscopic sensor made from graphene that is capable of detecting individual gas molecules such as NO_2, NH_3, H_2O, and CO. From the experiment, their sensor is able to respond as soon as a gas molecule attaches to or detaches from graphene's surface and the adsorbed molecules change the local carrier concentration in graphene. This leads to step-like changes in resistance.

The device shows concentration-dependent changes in electrical resistivity by adsorption of gases after which the sensor is regenerated by annealing at 150°C under vacuum. This ultrahigh sensitivity stems from the fact that pristine graphene is an exceptionally low-noise material. The detection limit for solid-state gas sensors is usually defined as the minimal concentration that causes a signal exceeding sensors' intrinsic noise. In Schedin *et al.* (2007) graphene sensor, a typical noise level in their devices is $\Delta\rho/\rho \approx 10^{-4}$ that translates into the detection limit of the order of 1 ppb. As a result, this places graphene on parity with other materials used for most sensitive gas sensors [98]. The lowest level of noise was found in their devices with the highest mobility (>10,000 $cm^2/V\,s$) and the lowest contact resistance. Sensors made from few-layer graphene (3 to 5 layers) were most electrically quiet, probably because their contact resistance could be as low as 50 Ω, as compared with typically 1,000 Ω for single-layer of graphene devices.

Different gases have different effects on the resistivity. The magnitudes and the sign of the change in the resistivity indicate whether the gas is an electron acceptor (*e.g.* NO_2, H_2O, and I_2) or an electron donor (*e.g.* CO, ethanol, and NH_3) [99]. Since conductivity is proportional to the product of number of charge carriers and mobility, the change in conductivity must be due to changes in the number density or mobility of carriers, or both. From the results, Hall effect measurement showed extra charge carriers being formed during gas adsorption on their device. That means that gas adsorption can increase the number of holes if the gas is an acceptor or increase the number of electrons if the gas is a donor. This change in the carrier concentration is the basic mechanism that governs the operation of all electrical conductivity-based graphene gas sensor devices towards the increased or decreased of resistance.

Graphene-based chemical sensors offer the possibility of ultrahigh sensitivity detection of a range of gas type in mixtures with air at room temperature and atmospheric pressure. Referring to Yavari and Koratkar (2012), comparing graphene to CNTs, it is concluded that a free-standing or suspended graphene sheet has both of its sides exposed to the chemical environment, thereby maximizing its sensitivity. But, for the multiwalled CNTs, the inner cylinders are shielded from the chemical environment. Even for SWCNTs, the ends may be closed (*e.g.* for tubes grown by CVD), or the metal contact pads might cap

the tubes and prevent the inside of the tube from participating in gas adsorption. Graphene also exhibits inherently low electrical noise at room temperature, which arises from its unique 2D crystal lattice and high electron mobility [100].

Chu *et al.* (2011) investigated the characteristics of hydrogen detection using epitaxial graphene covered with a thin layer of platinum as a catalyst. The multilayered graphene was grown by CVD on a Si-polar 4H-SiC substrate. Graphene covered with a thin film of Pt showed reduced resistance in response to exposure to 1% hydrogen at various temperatures. This sensor works based on splitting of the H_2 molecule in the presence of the catalytic metal. Dissociated hydrogen atoms will accumulate at the surface of Pt and diffuse into the graphene/Pt boundary, causing the hydrogen atoms to form covalent bonds with graphene. This hydrogenated form of graphene will have an increased work function and the separation distance increase between graphene and Pt can also cause the Fermi-level shift to become larger. Thus, the free carrier concentrations will increase and raise the conductance of the graphene/Pt device [101].

Chen *et al.* (2011) investigated the electrical resistivity of monolayer CVD-grown graphene that exhibits significant changes upon exposure to oxygen (O_2) at room temperature. Results showed that O_2 can be detected at concentrations of around 1.25% in volume ratio. When O_2 molecules are attached to the surface of graphene, they form epoxide and carboxylic groups that are electron-withdrawing and increase hole concentration of the conduction band which generates a significant decrease in resistance [102].

Unlike graphene with zero band gap, which greatly hinders its applications, penta-graphene (PG), a new 2D allotrope of carbon based on Cairo pentagonal tiling pattern, is a material with individual atomic layer exclusively consisting of pentagons (a mixture of sp^2- and sp^3-coordinated carbon atoms) in a planar sheet geometry [103]. The sensing capabilities of monolayer of PG using first-principles and non-equilibrium Green's function (NEGF) calculations towards small gas molecules, such as CO, CO_2, NH_3, NO, and NO_2, have been conducted by Cheng *et al.* (2019) [104]. The results proved that monolayer PG is most preferred for the NO_x ($x = 1, 2$) molecules with suitable adsorption strength and apparent charge transfer. Moreover, the current–voltage (I–V) curves of PG display a tremendous reduction of 88% (90%) in current after NO_2 (NO) adsorption. The superior sensing performance of PG rivals or even surpasses that of other 2D materials such as graphene and phosphorene. The ultrahigh sensitivity and selectivity to nitrogen oxides make PG a superior gas sensor that promises wide-ranging applications. Figure 7(a) shows that the a 3×3 PG supercell with and without gas adsorption is used for each of the left and right electrodes and the centre scattering region, respectively, and Figure 7(b) and (c) shows the I–V curves of PG with and without the NO_x gas adsorption.

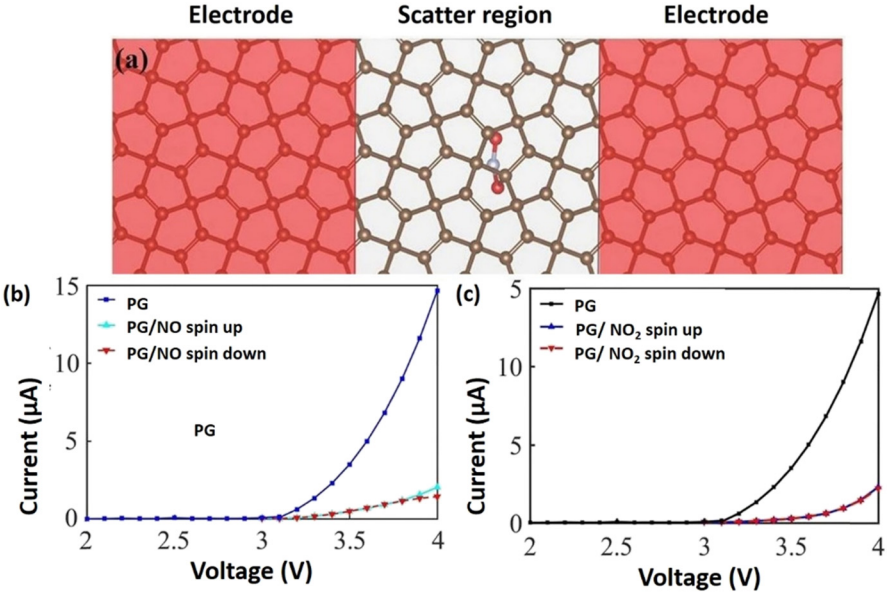

Figure 7: (a) Illustration of the two-probe systems of semi-infinite left and right electrode regions (red shaded region) which are in contact with the central scattering region of PG (b) and (c) display the I–V curves of PG and PG with the NO and NO_2 adsorption. Reproduced from ref. [104].

Lee *et al.* (2016) investigated the characteristic of defect-engineered graphene chemical sensors on NO_2 and NH_3 detection using commercial graphene [105]. Theoretically, a graphene defect engineering strategy was proposed to tailor the interface and mechanical properties of graphene nanocomposites. From the study, the defects were formed from the reaction of oxygen radicals and graphene *via* diffusion because the direct ion bombardment was blocked by the silicon wafer. During oxidation, oxygen radicals react with the carbon atoms in the graphene, forming sp^3-type defects and vacancies formed by the detachment of carbon atoms in the form of CO or CO_2. In this work, defects were created in graphene using oxygen plasma, with a conventional reactive ion etching system. The graphene was grown on copper foil by the CVD technique and the monolayered graphene ($0.5 \times 0.5\,cm^2$) on the copper foil was wet-transferred to the ($11\,cm^2$) SiO_2/Si substrate. Result shows that the defect-engineered graphene chemical sensors exhibited optimized sensitivities of 53 and 25% to 200 ppm of NO_2 and NH_3, respectively. The density functional theory simulations showed that the graphene sensors can be activated and enhanced by the presence of defects. Besides that, vacancy defect, whose density can be precisely controlled by defect engineering, is the main factor contributing to sensitivity. From the experiment, the pristine graphene exhibited sensitivity towards NH_3 molecules, suggesting that vacancies are already present even in pristine graphene. The lower adsorption strength of NH_3 compared with NO_2 can explain a higher sensitivity of the latter than the former. However, the increase in the sensitivity of NH_3 due to defect engineering was much higher than that in the sensitivity of NO_2 (increases of sensitivity for NO_2 and NH_3 gases were 33 and 614%, respectively) because there was no charge transfer between defect-free graphene and NH_3 molecules. Figures 8 and 9 show the molecular adsorption on defective graphene which has higher adsorption strength than pristine graphene for NO_2 and NH_3.

A developed graphene-based resistive gas sensor fabricated by transfer of CVD-grown graphene on a smooth paper showed low detection limit of 300 parts per trillion (ppt) for NO_2 at room temperature which is comparable to or better than those from other paper-based sensors [106]. The overall sensor response of the graphene paper sensor was around 118% ppm^{-1} of NO_2 and by ultraviolet exposure for 10 min, and the response is increased by a factor of 2.5. Referring to Kumar *et al.* (2015), large strain can generate cracks in graphene paper and results in large effect on its electrical and sensing properties. When graphene paper is subjected with different values of strain, the conductance (S) increased by a factor of 2 over the unstrained sample [106]. For large strains applied here (radius of curvature about 12 mm or lower), the resistance of the sample changes irreversibly to higher value of strains. Large strains can produce cracks and other defects in graphene layer, so this behaviour is expected. The cracks and defects formation provides more sites for adsorption of test gas, as well as bear large effect on resistance when they are bridged. As a result, the response improves as presented in the inset of Figure 11(c). Figure 10(a) and (b) shows the schematic diagram of preparation of graphene paper and the transfer process on the paper. Figure 11(a) shows the conductance change of graphene paper strips when 2.5 ppm of NO_2 exposure, while Figure 11(b) shows the change in conductance of a graphene paper as concentration of NO_2 increases from 0.5 pm up to 2.5 ppm.

Graphene gas sensors with different number of graphene layers were successfully fabricated by the facile

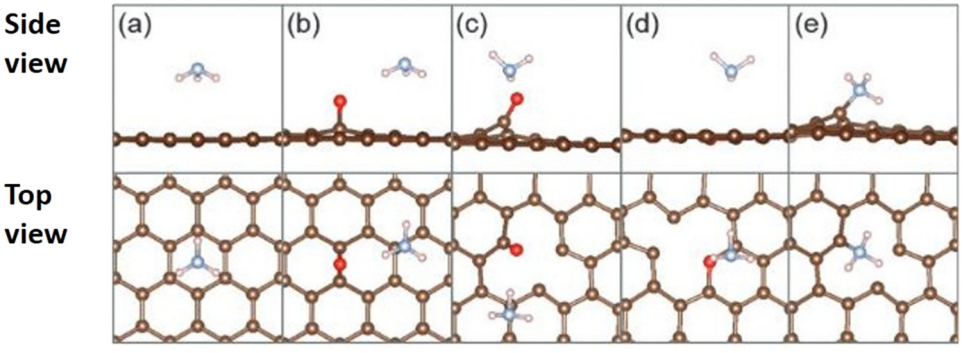

Figure 8: Optimized structures of the NO_2 molecule adsorbed on (a) pristine graphene, (b) sp^3-type defect (epoxy group)-graphene, (c) sp^3-type defect (carbonyl group)-graphene, (d) sp^3-type defect (ether group)-graphene, and (e) single vacancy of graphene. The red, brown, and grey colours represent O, C, and N atoms, respectively. Reproduced from ref. [105].

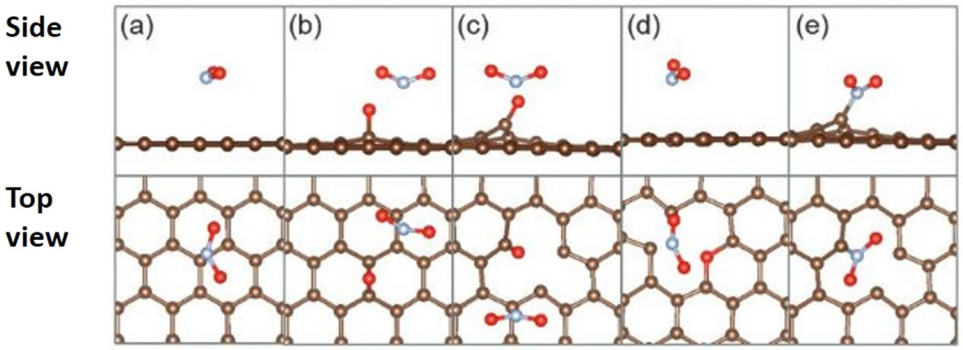

Figure 9: Optimized structure of the NH_3 molecule adsorbed on (a) pristine graphene, (b) sp^3-type defect (epoxy group)-graphene, (c) sp^3-type defect (carbonyl group)-graphene, (d) sp^3-type defect (ether group)-graphene, and (e) single vacancy of graphene. The red, brown, grey, and light pink colours represent O, C, N, and H atoms, respectively. Reproduced from ref. [105].

transfer of monolayer CVD graphene sheets grown on Cu foil for NO_2 sensing detection [107]. Results on gas sensing show that all graphene sensors demonstrated the p-type sensing behaviours under the adsorption of NO_2 molecules. The highest response and the highest sensitivity towards NO_2 at room temperature were shown by the bilayer graphene gas sensor. The increase is linearly with NO_2 concentration over the range of 1 to 25 ppm and had a high linear sensitivity of 1.409 ppm^{-1}. The bilayer graphene gas sensor also exhibited high selectivity to NO_2 against CO, CO_2, NH_3, C_2H_5OH, and H_2 at room temperature.

For the NO_2 sensing mechanism, p-type gas sensing characteristics and bilayer graphene display considerably higher NO_2 response than monolayer, 3-layer, and 4-layer of graphene. The NO_2 sensing mechanism of graphene at low temperature may generally be explained based on (1) reducing reaction and (2) direct change transfer processes. In the case of the reducing reaction process, chemisorbed oxygen species (O_2^-) could be formed on graphene surface even at low or room temperature. NO_2 may react with O_2^- to generate NO, O_2, and electrons. Yet, due to insufficient activation energy, this reaction should not occur at low temperature, below 100°C [107]. Thus, direct charge transfer process appears to be the most probable dominant process for NO_2 sensing of graphene gas sensor at room temperature. The direct charge transfer occurs between NO_2 molecules and graphene surface when NO_2 molecules are adsorbed on the graphene surface as NO_2^- by chemisorption.

Before the NO_2 gas adsorption, the monolayer of graphene at Figure 12(a) exhibits the unique massless conical band electronic structure, while bilayer and multilayer graphene structures have typical parabolic bands

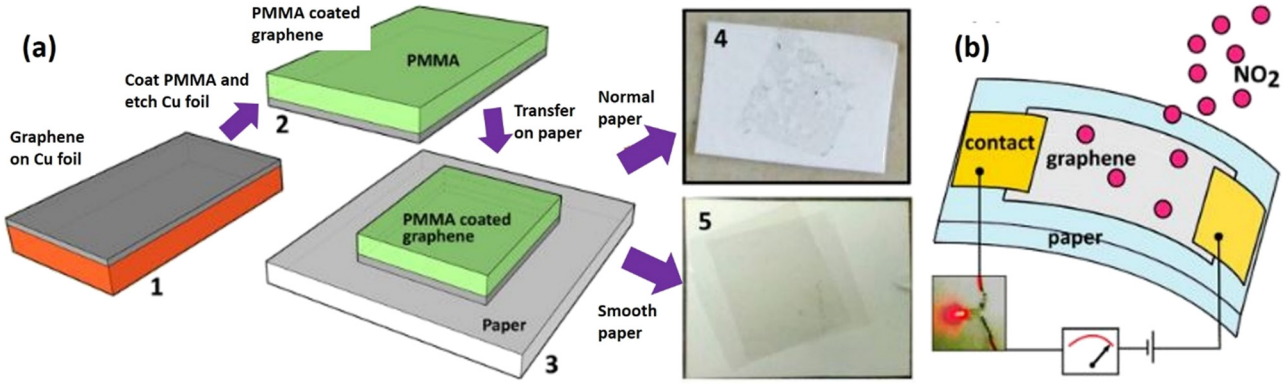

Figure 10: (a) and (b) Schematic diagram of graphene transfer process on to the paper. Starting with (1) graphene on Cu foil, (2) a layer of poly(methyl methacrylate) (PMMA) is spin-coated and Cu is etched to get graphene supported by PMMA in water, (3) PMMA-graphene film is then dredged on to paper and PMMA is dissolved with acetone and (4) normal paper yields patchy coverage compared to transfer on smooth paper (5). The smooth paper at (5) shows two layers of graphene transferred on smooth paper. (b) Schematic of a G-paper strip in action as a gas sensor. The circuit had sufficient current to make an LED glow ((bottom left). Reproduced from ref. [106].

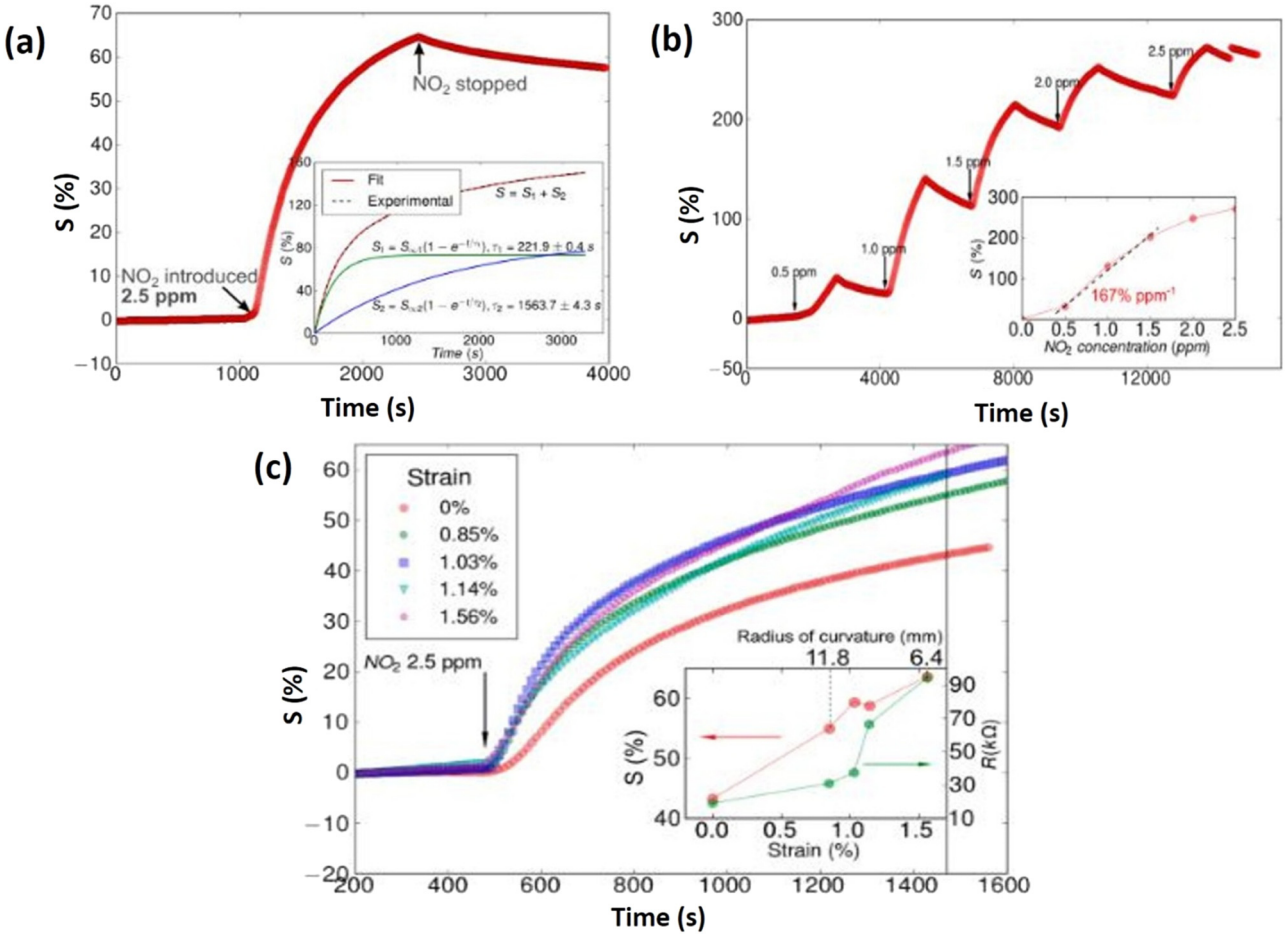

Figure 11: (a) Change in conductance of a graphene paper strip to 2.5 ppm of NO_2. The inset shows a fit of double exponential function to the temporal response for 2.5 ppm of NO_2, (b) change in conductance of a graphene paper as concentration of NO_2 increases starts from 0.5 to 2.5 ppm. The inset shows the plot of response at t = 1,000 s vs the concentration of NO_2, which has a slope of 167 ppm^{-1} at the start (indicated by dashed line) and (c) change in conductance of a graphene paper as strain is applied at 2.5 ppm of N NO_2 flow. The inset shows that both the baseline resistance and response of the strip increase with increasing strain. Reproduced from ref. [106].

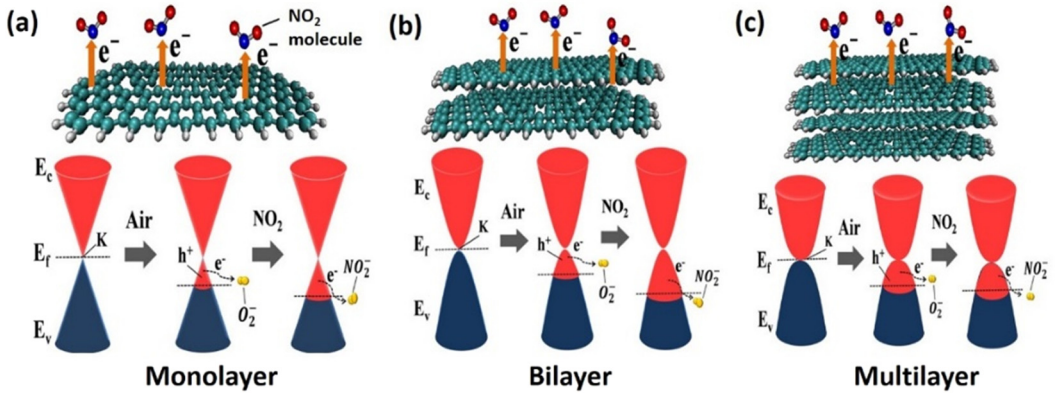

Figure 12: Schematic diagram of band diagrams of NO_2-sensing mechanism of (a) monolayer, (b) bilayer, and (c) multilayer of graphene gas sensors proposed by Seekaew *et al.* Reproduced from ref. [107].

associated with the finite charge carrier effective mass, which increases with increasing number of graphene layers [107]. In air, O_2^- species adsorbed on graphene surface at room temperature will accept electrons from the valence band of graphene, inducing holes and p-type conductivity. In addition, the amount of holes will increase with increasing number of graphene layers because more electronic states are available in the wider valence bands of bilayer and multilayer graphene, leading to lower p-type electrical resistivity (Figure 12(b) and (c)). This explains large decrease of resistance with increasing the number of graphene layers. Upon exposure to NO_2, NO_2 molecules are adsorbed on graphene as NO_2^- extracts more electrons from the valence band [108] which leads to the increase of hole density, the lowering of Fermi level, and increase of p-type conductivity of graphene sensitivity [109].

For monolayer graphene at Figure 12(a), the amount of charge transfer to NO_2 molecules may be quite limited due to less available electronic state at high energy in valence band compared with bilayer one. Thus, the bilayer graphene, which has comparable accessible active surface area as monolayer one, could exhibit more charge transfer due to NO_2^- adsorption leading to a larger change in resistance and higher NO_2 response. Then, when the number of graphene layers is increased, the relative amount of transferred charges will be reduced substantially since NO_2 molecules can only extract electrons from graphene surface, while there are very large number of hole charge carriers internally present in multilayer graphene (the low resistance value about 60 Ω for 4 graphene layers) which leads to small increase of p-type conductivity and low NO_2 response for multilayer graphene. Figure 12 shows the schematic diagram of band diagrams of NO_2-sensing mechanism of (a) monolayer, (b) bilayer, and (c) multilayer graphene gas sensors.

3.2 Performance of GO nanocomposite-based sensor

As discussed in synthesis of graphene in Section 2, the chemical oxidation of graphene and simultaneous reduction of resulting GO is one of the popular approaches used for graphene synthesis. GO has a layered structure parallel to graphene, but it is functionalized with oxygen-containing groups such as hydroxyls, epoxies, carboxyl, and lactones. These functional groups not only expand the interlayer spacing, but also make the atomic-thick layers more hydrophilic, enabling these oxidized layers to exfoliate in water under ultra-sonication or mechanical stirring [110]. Choi *et al.* (2015) studied the role of oxygen functional groups in GO for reversible room-temperature NO_2 sensing [111]. Based on the results, graphene-based materials' defects such as oxygen functional groups, Stone-Wales defects, and holes from the basal plane can act as active sites for interaction with molecules [112]. Owing to its oxygen-rich functional groups, GO could be considered as an ideal material for gas sensing. But the numerous oxygen functional groups of GO make it too electrically insulating for use as an active material for chemiresistive sensors. Choi *et al.* (2015) also stated that the major drawback of rGO-based sensors is the extremely sluggish and irreversible recovery to the initial state after a sensing event, which makes them incapable of producing repeatable and reliable sensing signals.

Based on study by Peng and Li (2013), GO shows better detection of NH_3 than pristine graphene, since the active surface of defective sites of GO such as the epoxy and hydroxyl groups promotes the interactions between the NH_3 molecules and GO [113]. Based on *ab initio* studies [114], the presence of hydroxyl and carbonyl groups attached on the carbon atoms on GO surface results in large binding energies and enhanced charge transfers from nitrogen oxides NO_x (x = 1, 2, 3). This leads to chemisorption of gas molecules on GO surface [115]. Alam *et al.* (2018) have studied the development of GO-gold nanocrystals (AuNCs) nanocomposite-modified glassy carbon electrode (GCE) for the sensitive detection of dopamine (DA), uric acid (UA), and 4-aminophenol (4-AP) [116]. The GO was synthesized through modified Hummer's method, which was utilized to prepare GO-AuNCs nanocomposites by *in situ* synthesis method using sodium L(−) malate as a reducing agent. It was observed that the sensor showed interference-free and selective detection of DA and UA with sensitivities of *ca.* 30.3 and 17.28 μA/cm^2/μM, respectively, and detection limits of *ca.* 28 and 50 nM, respectively, with wider dynamic ranges, measured by differential pulse voltammetry (DPV) technique. It also shows a sensitivity and detection limit of *ca.* 5.70 μA/cm^2/mM and 0.017 nM, respectively, for the detection of 4-AP, using current density (J)-voltage (V) measurement method. The sensor revealed an excellent stability, reproducibility, and recoveries of DA, UA, and 4-AP in real samples.

Yu *et al.* (2018) had fabricated Pt nanoparticle-incorporated GO nanocomposite-based microfiber sensor with high sensitivity for NH_3 sensing [117]. The Pt-decorated sensor displayed a sensitivity of 10.2 pm/ppm, 3 times higher than the sensitivity without Pt-decorated nanoparticles. These results indicate the sensor has the optimal sensing sensitivity when the Pt nanoparticle concentration

is 185.2 mg/L and exhibits a linear response with NH_3 gas concentration below 80 ppm. This nanocomposite film-based passive optical fibre sensor provides an approach for highly sensitive NH_3 sensing in a limited space, flammable or in explosive environment.

An excellent gas sensing characteristic of GO is contributed by the dangling bonds attached on its surface, which are essential for detecting the gas molecules. Yu and team (2018) made GO sheets that have higher adsorption efficiency of gas molecules by the presence of Pt nanoparticles. More NH_3 gas molecules absorb to the surface of GO because the NH_3 gas molecule can bind strongly to the bulk surfaces of platinum [118]. This incidentally improves the absorption ability of GO to NH_3 gas molecules, resulting in the improvement in sensitivity for NH_3 sensing. From their experiment, the different concentrations of Pt with the same GO content were tested for NH_3 sensing. The result shows that the sensitivity for NH_3 sensing is raised as the Pt concentration increases in the range from 0 mg/L to 185.2 mg/L. The sensing sensitivity was not improved significantly when the Pt concentration exceeds 185.2 mg/L. This could be because the refractive index change of GO is saturated with more gas molecules absorbed onto the surface of GO.

NH_3 gas sensor characteristics based on fluorinated-GO (f-GO) have been investigated by Park *et al.* (2016) [119]. Gas sensor was fabricated by dropping dispersion solution (5 µL) of f-GO onto SiO_2/Si wafers patterned with Pt electrodes. The fluorination treatment was carried out at partial fluorine gas (98%) pressures of 0.1 (GO-F1N9), 0.3 (GO-F3N7), and 0.5 (GO-F5N5) bar with an injection time of 5 min. The total pressure was adjusted to 1 bar with nitrogen gas, and the reaction time was 10 min. After the reaction, the residual gas was expelled and then purged 2 times with nitrogen gas. The gas sensor fabricated using f-GO (GO-F1N9) shows an approximately 7% change in the resistive response, whereas the non-treated GO does not exhibit any sensing ability to NH_3 gas [119]. This change in the response is attributed to the lower Fermi level of GO and the increased number of holes in the GO after fluorination, which is helpful for effectively attracting NH_3 gas. However, all samples do not exhibit recovery at room temperature and the presence of a higher number of fluorine-carbon bonds caused a decrease in the electrical resistance change.

For these reasons, fluorine bonded to GO surface leads to change in the electronic structure of GO. In Park *et al.* (2016) study, f-GO acts as an electron acceptor showing an increase of resistance when the reducing gas like NH_3 is detected (Figure 13). GO decorated with fluorine functional group has a lower Fermi level than

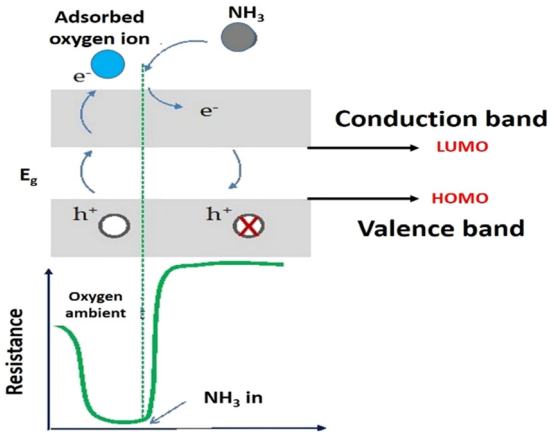

Figure 13: Adsorption phenomenon of NH_3 with increase of resistance when the reducing gas like NH_3 is detected.

raw GO and makes electrons in the valence band move to the lowest unoccupied molecular orbital (LUMO) due to high electronegativity of fluorine. This fluorine doped on the GO surface creates a higher number of holes in the valence band. The absorption of NH_3 gas on f-GO results in the electron lone pair of the NH_3 molecules being transferred to LUMO of f-GO, leading to increases of Fermi level. Holes are not created in the valence band any more, thus the current flow is limited by the increase of resistance due to the decreased number of hole carriers. However, the GO-F5N5 (the higher fluorine gas pressure bar) showed a lower sensitivity to NH_3 relative to those of GO-F1N9 and GO-F3N7. This result is supported by the loss of sp^2 bonds by excess fluorination in GO. Figure 14 shows the sensing behaviour of f-GO under 100 ppm of NH_3 gas at room temperature.

Prezioso *et al.* (2013) had investigated a number of forms of GO to optimize the sensing sensitivity and efficiency [120]. The fabricated sensing device by drop-casting water-dispersed single-layer GO flakes on standard 30 µm spaced interdigitated Pt electrodes. A practical p-type gas sensor using GO drop-casted shows a stable operating conditions, has a lifetime larger than 1,000s h, and exhibits a very low detection limit (20ppb). This excellent performance is due to the high quality of GO which have large and highly oxidized flakes. With correspondence to other carbonaceous materials such as rGO and CNTs, GO has the advantage to have a much larger number of active sites but the limitation being poorly conductive. Because of this, GO is considered as a good choice for applications that do not require fast responses, but require high sensitivities.

Dielectrophoresis (DEP) process for GO nanostructures for hydrogen gas sensor at room temperature was investigated by Wang *et al.* (2014) [121]. The GO

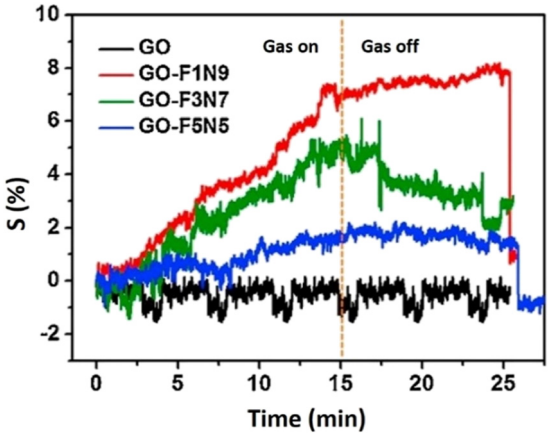

Figure 14: Sensing behaviour of f-GO under 100 ppm of NH_3 gas at room temperature. Reproduced from ref. [119].

nanostructures synthesized using Hummer's method was assembled into gold electrodes using DEP process by varying parameters such as frequency, peak-to-peak voltage (V_{pp}), and processing time (t). Results show that an optimum DEP parameter required for hydrogen gas sensing using GO nanostructures is observed to be $V_{pp} = 10$ V, frequency = 500 kHz, and $t = 30$ s. The optimized device was found more effective and better hydrogen sensor with a good sensing response of 5%, fast response time (<90 s), and fast recovery time (<60 s) for 100 ppm hydrogen gas concentration at room temperature.

Some *et al.* (2013) had studied the highly sensitive and selective gas sensor using hydrophilic and hydrophobic graphenes coated on polymer optical fibre (POF) [122]. The high oxygenated functionalities on GO surface were observed to maintain the high sensitivity in highly unfavourable environments (extremely high humidity, strong acidic or basic). The GO-based sensor displayed faster sensing and higher sensitivity when compared to rGO even under extreme environments of over 90% humidity, making it the best choice for an environmentally friendly gas sensor. Furthermore, according to the experimental results, the sensitivity of GO to VOCs (mainly nitro and amine containing compounds) is much higher than that of rGO due to the presence of numerous polar functional groups like hydroxyl and carboxylic acid [122].

Shown in Figure 15 are the comparison of sensing responses for GO and rGO to eight different chemicals (hydrazine, ethanol, methanol, dichloromethane, acetone, THF, nitromethane, and diethylamine) at a 500 ppb of concentration level. The result shows that only GO and only rGO-coated POF sensors showed different sensitivities toward the various vapours. The intensity of the reflected optical response for the only GO and only rGO POF sensor was highest for hydrazine, diethylamine, and nitromethane vapours at the same concentration, respectively and was lowest for methanol and dichloromethane vapours, respectively. The experimental result shows the sensitivity of GO to VOCs (mainly nitro and amine containing compounds) is much higher than that of rGO due to the presence of numerous polar functional groups.

3.3 Performance rGO nanocomposite-based sensor

Referring to Yavari and Koratkar (2012), even though GO is electrically insulating due to plentiful oxygen functional groups, the conductivity can be restored to several orders of magnitude. This is by the removal of oxygen groups using chemical or thermal reduction or can be partially reduced to graphene-like sheets. By removing the oxygen-containing groups with the recovery of a conjugated structure termed as rGO, the conductivity can be possessing up to several orders of magnitude. Even so, this process does not lead to pure graphene, and some residual oxygen groups remain even after the reduction process. Consequently, rGO has both high electrical conductivity and chemically active defect sites, making it a promising candidate for gas sensing. This sensor is able to reversibly and selectively detect chemically aggressive vapors such as NO_2, Cl_2, and so forth down to concentrations ranging from 100 to 500 ppb [13].

Exploitation of a new concept for enhancing the performance of rGO gas sensors by combining the structural engineering techniques of 3D microstructuring has been

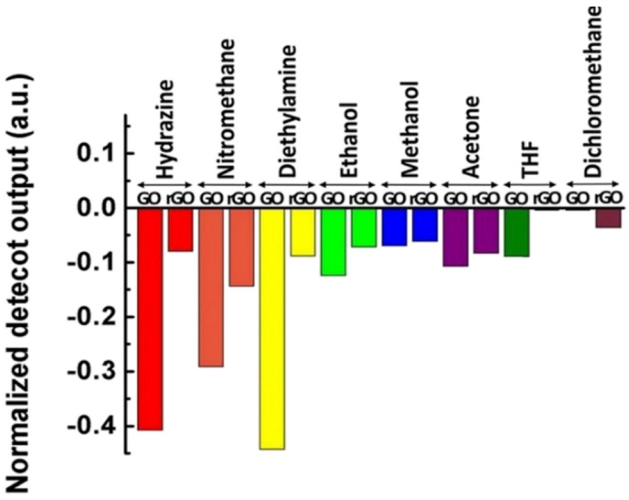

Figure 15: Comparative of sensing behaviour towards the different chemical gas by GO and rGO coated on POF. Reproduced from ref. [122].

explored by Duy *et al.* (2015) [123]. From that, a high performance of three-dimensional chemical sensor platform using rGO for NH_3 and NO_2 detection was achieved. The performance of a chemical sensing device was enhanced from a simple three-dimensional (3D) chemiresistor-based gas sensor platform with an increased surface area by forming networked, self-assembled rGO nanosheets on 3D SU8 micro-pillar arrays. The 3D rGO sensor is highly responsive at low concentration of NH_3 and NO_2 diluted at room temperature. Compared to the two-dimensional (2D) planar rGO sensor structure, as the result of the increase in sensing area and interaction cross-section of R-GO on the same device area, the 3D rGO gas sensors show improved sensing performance with faster response (about 2%/s exposure), higher sensitivity, and even a possibly lower limit of detection towards NH_3 at room temperature. Figure 16 shows the schematic diagram of structure for 2D and 3D devices and sensing response of rGO sensors towards 5 ppm of NO_2 and 40 ppm of NH_3.

A sono-synthesis method to produce rGO nanosheets for NH_3 vapour detection at room temperature was studied by Veluswamy *et al.* (2015). From their study, the polyethylenimine (PEI) was used as reducing agent to reduce the GO, which increases the conducting nature of the GO. The synthesis of GO and reduced rGO was prepared by Hummer's method and sonication method with low-frequency ultrasound under ambient condition, respectively. The rGO-based chemiresistive sensors showed a good sensing response (3,500%), high sensitivity (38.85 kΩ/ppm), low level detection (1 ppm), wide range of detection (1 –100 ppm), quick response (6 s), recovery time (75 s), good reparability, better selectivity, and stability to be operated at room temperature for NH_3 detection. Figure 17(a) shows the sensing response of various test vapours, and Figure 17(b) and (c) shows the sensing response of rGO film towards 1–5 ppm, and 10–100 ppm range of NH_3 vapour [124].

The NH_3 sensing response of GO and rGO also has been investigated by Veluswamy *et al.* (2018) and shown in Figure 18. The result indicates that the NH_3 response increases for rGO drastically (nearly 3–9 times), increases from 16 to 45% for 10 ppm, and from 403 to 3,400% for 100 ppm for rGO. The oxidation process from graphene to the highly oxygenated GO depends on various factors such as the size of GO sheets, the content of oxygen functional groups, and thus greater defect intensity of GO, which is confirmed by Raman results [125]. The electrical

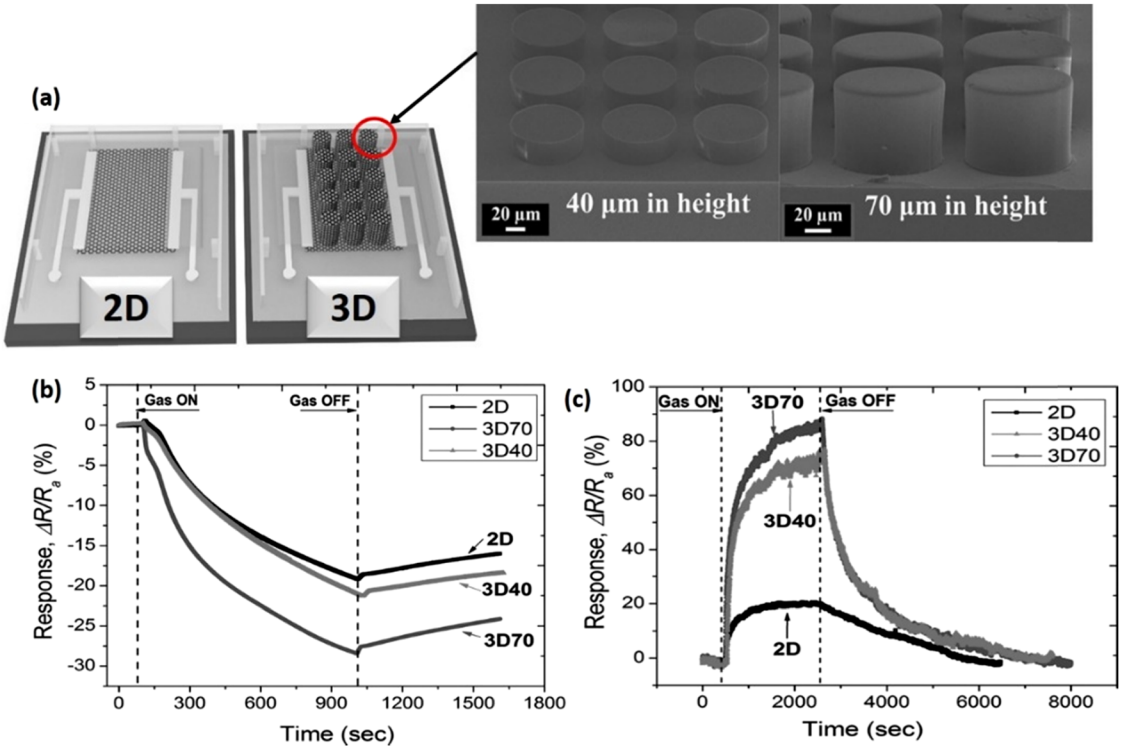

Figure 16: (a) Schematic diagram of structure for 2D and 3D devices of SU8 micro-pillar arrays with different heights of 40 and 70 µm for 3D devices, (b) sensing response of rGO sensors towards a) 5 ppm NO_2 (exposure time about 15 min) and (c) 40 ppm NH_3 (exposure time about 30 min). Adapted from ref. [123].

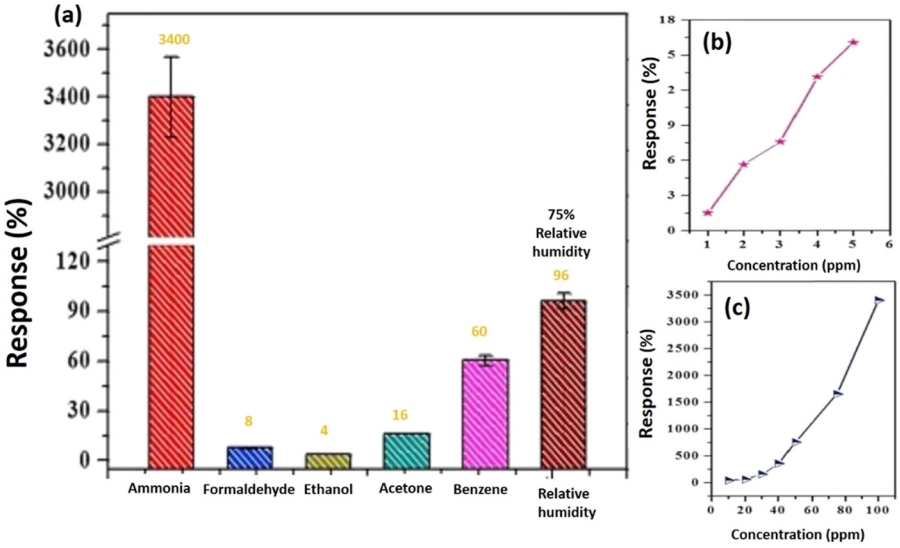

Figure 17: (a) Sensing response of various test vapours, (b) and (c) show the sensing response of rGO film towards 1–5 ppm and 10–100 ppm range of NH_3 vapour. Adapted from ref. [124].

resistance of GO is high because of the disturbance of the conjugated electronic structure by these oxygen-containing groups. However, chemical reduction of GO can effectively bring back its conductivity; meanwhile, a fewer amount of oxygen-containing functional groups still remain in rGO, because of its incomplete reduction. The reduction process may introduce some vacancies and structural defects which can also act as adsorption sites. From that, the interaction of chemical molecules with high-energy defects in graphene differed dramatically from those with conjugated carbon structure. Therefore, optimization of defect density and its kind may be an effective way to manage the response, sensitivity, and selectivity of rGO-based chemical sensor [125].

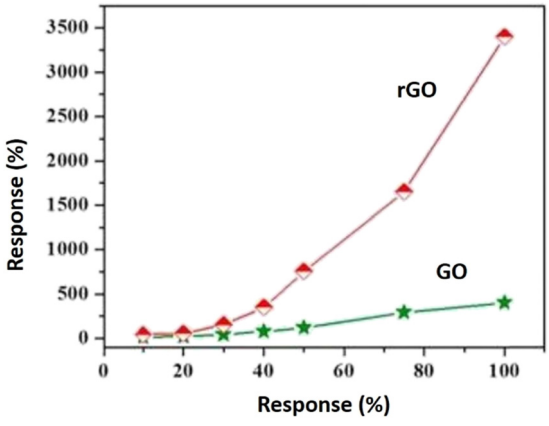

Figure 18: Comparative ammonia sensing response of GO and rGO film. Adapted from ref. [124].

A highly selective detection of carbon monoxide (CO) gas by rGO-based chemical sensor at room temperature has been investigated by Panda *et al.* (2016) [126]. The sensing performances of rGO-based chemical sensor against CO were studied in terms of percent sensitivity (sensor response), response and recovery times, and I/V characteristics at room temperature. Gas sensing experiments exhibit about 71% sensitivity at room temperature at 30 ppm of CO. The selectivity of the sensor using different n-type reducing gases was negligible cross-sensitivity against NH_3, CH_4, and H_2 at different concentrations. Thus, the rGO is shown as highly potential material for development of CO gas sensor with high degree of sensitivity, selectivity, and reliability, proving it selective to CO gas at room temperature within permissible exposure limits.

The research on rGO-based gas sensor functionalized with a peptide receptor to detect explosives, dinitrotoluene (DNT), which is a by-product of trinitrotoluene (TNT) was investigated by Lee *et al.* (2019) [127]. The rGO-based sensor was fabricated using DNT-specific binding peptide functionalized rGO. The sensitivity was calculated by measuring the resistance change using the differential signals between DNT-BP (binding peptide) and DNT-NBP (non-binding peptide) to function as highly specific and highly non-specific (for the control experiment) peptide receptors.

The rGO-based sensor showed an excellent linear sensitivity of $(0.27 \pm 0.02) \times 10^{-4}$ ppb with an approximate limit of detection (LOD) of 2.43 ppb. The multi-arrayed rGO sensor was fabricated using spin coating

and a standard microfabrication technique. The result was sensitivity of 27 ± 2 × 10^{-6} part per billion (ppb) for the slope of resistance change versus DNT gas concentration of 80, 160, 240, 320, and 480 ppm, respectively. By sequentially flowing DNT vapour (320 ppb), acetone (100 ppm), toluene (1 ppm), and ethanol (100 ppm) onto the rGO sensors, the change in the signal of rGO in the presence of DNT gas is 6,400 × 10^{-6} per ppb (Figure 19(c)). However, the signals from the other gases show no changes and represent highly selective performance. Figure 19(a) and (b) shows the rGO-based sensor for DNT detection and location of the rGO sensor patterns (200 µm × 100 µm) between the Au electrodes, respectively.

A rGO-based sensor was synthesized and fabricated under H_2/Ar treatment 100 to 900°C for H_2 detection [128]. Before that, the GO samples were prepared according to a modified Hummers' method. The prepared GO was then treated at different temperature to obtain a series rGO samples (rGO-100 to rGO-900); numbers denote the treating temperature. From the results obtained, the rGO-100 and rGO-200 showed very weak responses. Further responses of rGO-300 to rGO-900 against 500 ppm of H_2 at room temperature were presented in Figure 20(a). From that, rGO-300 had exhibited the best sensitivity towards the H_2 detection. Other than that, CO and CH_4 also produced signals on rGO-300-based sensors. The balance between the chemical adsorption capacity and electronic conductivity and the dominance of either electrons or holes are the key factors of the high sensitivity from the rGO-300.

Zhang *et al.* (2011) stated that in order to generate a strong sensing signals, adsorption of target gas molecules was necessary. It required relatively strong binding force between the sensing materials and the target gas molecules. As example, it was reported that the hydrogen molecules tended to be adsorbed on the defect site of the rGO (Figure 20(a)). Thus, the binding force between H_2 and the sidewall of rGO was rather weak. This was the same for rGO-700 and rGO-900 samples because these two samples had few defect sites. For rGO, the oxygenate groups could be considered as the defect sites on the graphene sheets. The relationship among sensing properties, conductivity, and the oxygen content could be further described in Figure 20(b). The oxygen content decreased from GO to rGO-900 as determined from XPS, leading to increased conductivity. During the sensing process, the gas molecule is adsorbed on the rGO surface with the oxygenated groups through hydrogen-bonding, then electron is transferred to the rGO resulting in a change of the resistance. In order to generate a sufficient sensing signal, a sufficient amount of functional groups is needed to act as an adsorption site. However, too many functional groups also would significantly reduce the conductivity of the rGO sample as observed on rGO-100 and rGO-200. The amount of hydrogen adsorption may also affect the response pattern of rGO-300 and rGO-900. Therefore, a delicate balance between chemical adsorption capacity and the conductivity of the rGO samples was the key factor for good sensing responses' properties realized on rGO-300.

Lipatov *et al.* (2013) had fabricated an array of thermally rGO-based integrated gas sensors [129]. The result shows the definitive identification of chemically similar analytes such as ethanol, methanol, and isopropanol by

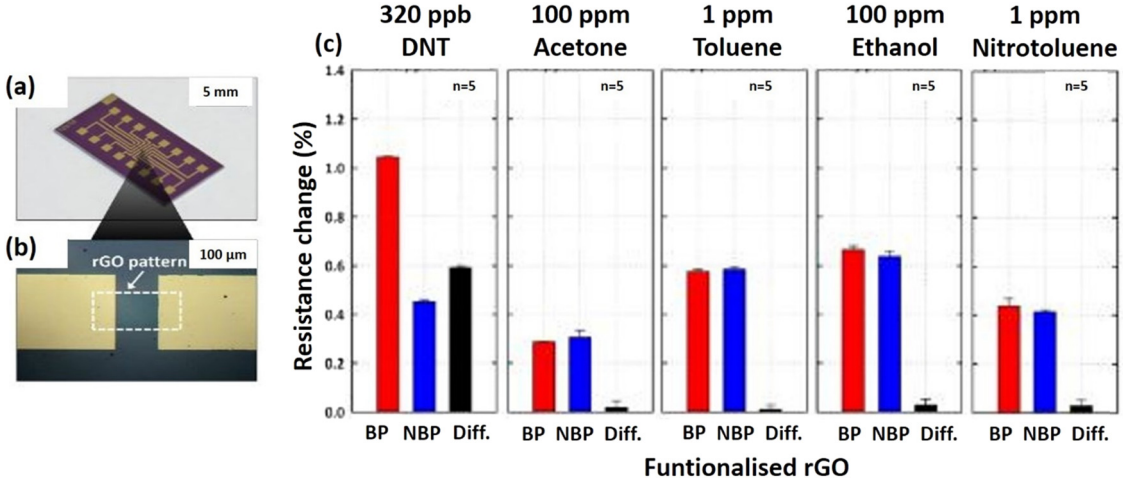

Figure 19: (a) Enlarged rGO chemical sensor with eight multiple arrays for DNT detection, (b) location of the rGO sensor patterns (200 µm × 100 µm) between the Au electrodes, and (c) resistance change on five different gases: the differential values (black bar) of DNT-BP and DNT-NBP confirm the high selectivity. Adapted from ref. [127].

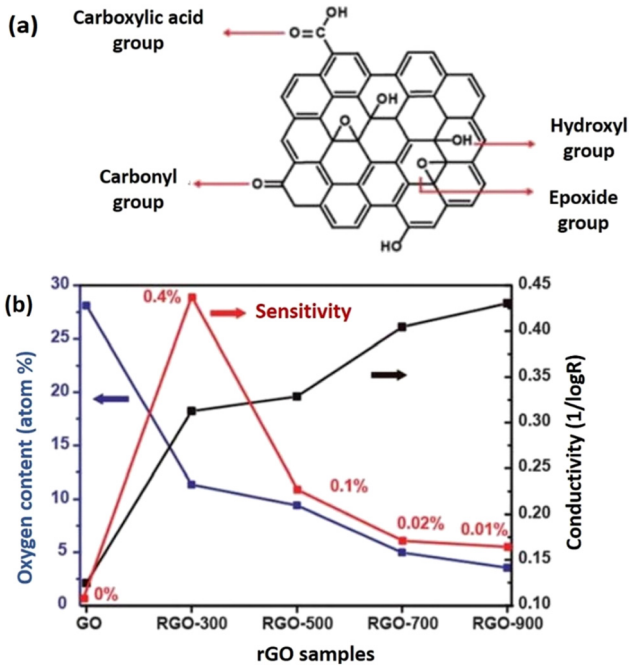

Figure 20: (a) rGO structure with the attached carbonyl, carboxylic, hydroxyl, and epoxide groups considered as defective sites and (b) oxygen content, conductivity, and sensitivity of rGO samples with different treatment temperature. Adapted from ref. [128].

making use of the significant device-to-device variations of rGO-based sensors. Each rGO device used in the integrated gas sensing system has a unique sensor response due to the irregular structure and electronic properties of the rGO flakes produced from the same fabrication process. The sensing behaviour for rGO-based sensor arrays demonstrated a high selectivity that was sufficient to discriminate between different alcohols, such as methanol, ethanol, and isopropanol, at a 100% success rate (Figure 21). According to Robinson *et al.* (2008), the fast response for a certain gas or chemicals could be attributed to the adsorption of molecules at the low-energy binding sites, such as sp^2 carbon domains, while the slow response was mainly caused by interactions between gas molecules with high-energy binding sites, such as vacancies, defects, and oxygen-containing functionalities [130].

3.4 Performance of hybrid graphene/metal oxide nanocomposites-based sensor

Widely used commercial gas sensors are primarily focused on the semiconductor of metal oxide, polymer materials, and various sensing methods: optical, calorimetric and acoustic methods, and gas chromatography approaches. The shortcomings of these gas sensors can be one or more: expensive, rare ppb sensitivity, poor selectiveness, low endurance, poor reproducibility, difficult miniaturization, and high power consumption [45]. However, higher operating temperatures of these sensors obviously negatively affect the integration and long-term stability of the device, resulting in high power consumption as well as environment pollution as explosive gases may be emitted. Thus, a combination of graphene with metal oxide is one of improved strategies in order to overcome the hindrances.

To date, owing to their superior stability and as their electrical resistance to adsorbates is relatively highly sensitive, various kinds of metal oxides like n-type zinc oxide (ZnO) [131], iron(III) oxide (Fe_2O_3) [132], stannous oxide (SnO_2) [133], Indium oxide (In_2O_3) [134], tungsten oxide (WO_3) [135], and p-type metal oxide like copper(II) oxide (CuO) [136], nickel(II) oxide (NiO) [137], chromium (III) oxide (Cr_2O_3) [138], cobalt(II,III) oxide (Co_3O_4) [139], *etc.* have been extensively explored as gas sensing materials. Figure 22(a) shows classification of n-type and p-type of metal oxide used as chemical sensor and Figure 22(b) shows results of a search study on metal oxides semiconductor used as sensing materials for chemoresistive gas sensors, including both the n-type and p-type oxides [140].

Due to their intrinsic large surface area, high electron mobility, and excellent conductivity under ambient conditions, rGO as derivatives of graphene are considered as ideal candidate in developing a room temperature gas like NO_2 gas sensors. rGO are more practically applied to realize room-temperature gas sensing in view of their cost-effective mass production and the introduced oxygen functional groups and surface defects, which act as active sites for interaction with gas molecules. Thus, it is especially important to combine graphene and metal oxides to form hybrid nanostructures, since they do not only show the different properties of nanoparticles and graphene, but also display additional synergistic effect of being attractive, favourable for gas sensor applications, and foremost for the detection of gas at room temperature [141].

Due to adsorption of contaminants such as water and oxygen molecules, graphene and rGO comprised a bipolar and nearly symmetrical behaviour in the electron and hole doping regions. Hence, they show p-dominant (hole carriers) conducting properties. In addition, the decoration of graphene sheets with an n-type metal oxide can result in forming of a p–n junction, which exhibits better performances than the individual materials, resulting in new nanostructure. Researchers have therefore paid a great

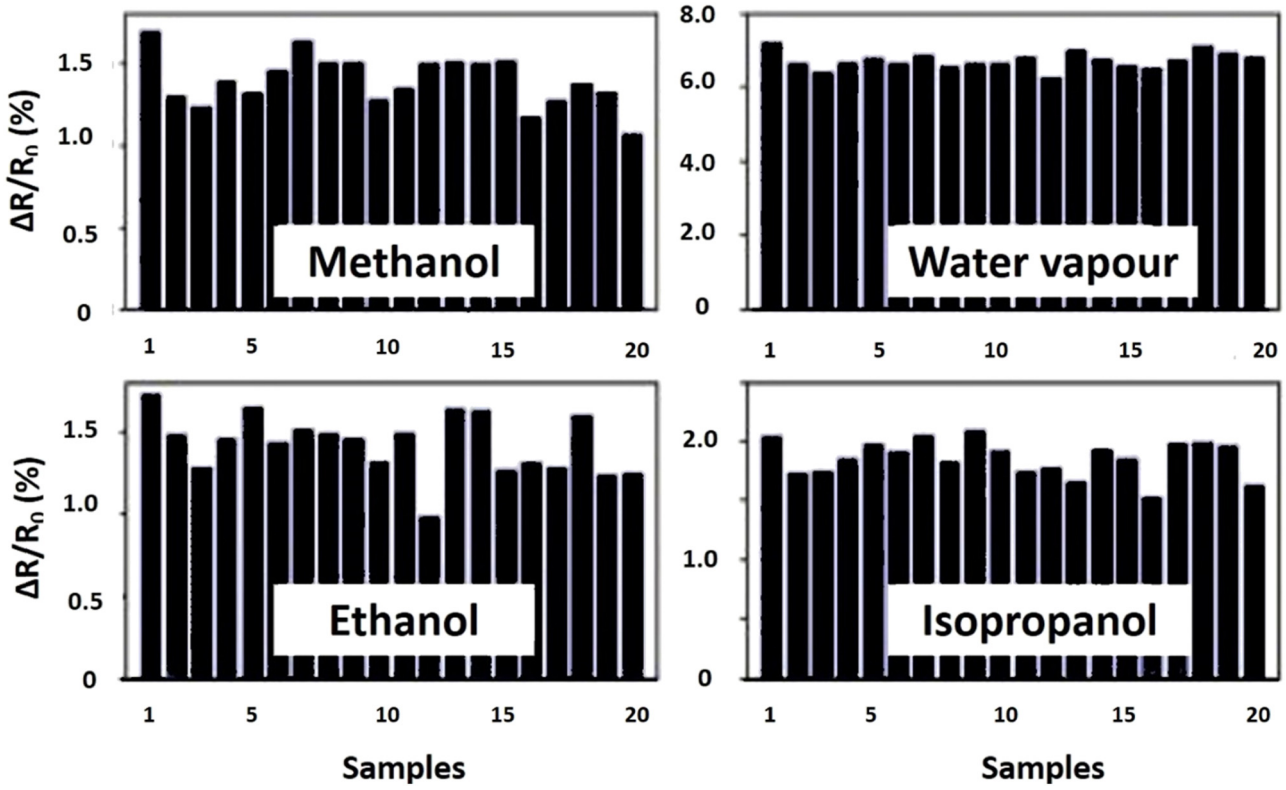

Figure 21: Scatterings of gas responses from twenty samples of rGO-based sensor to different analytes with 100% success rate at 1,000 rpm. Adapted from ref. [129].

deal of attention in recent years to graphene hybridized with metal oxide or hybrid rGO architectures that function at room temperature for very sensitive, selective, and cost-effective gas sensors [142–145].

Spinel Co_3O_4 is a type of metal oxide consisting of CoO and Co_2O_3 which are rich in oxygen content, and thus comprised semiconductor features of p-type have been studied as a potential gas sensing material. The gas sensing characteristics have been investigated, where the sensing is normally based on the catalytic properties of the oxide surface and typically operating sensors at temperature over 200°C [146–148]. Chen *et al.* (2013) observed that the rGO-based NO_2 gas sensors could considerably improve their reaction at room temperature when the Co_3O_4 nanocrystals are intercalated [149]. Two particular mechanisms clarified the improved response of Co_3O_4 graphene sensor in Co_3O_4 bonds efficiently to a single rGO layer surfactant, resulting in stronger reaction than pure rGO, with an expanded surface area. In addition, the Co_3O_4 nanocrystals act like nanopillars resulting in an extra macroporous arrangement between the layers of rGO, thereby further improving the gas diffusion to the surface of rGO, driven by the capillary forces [150]. Second is the hybridizing effect between the Co element and GNR as proposed by Liang *et al.* [151], suggested to help in improving the ability to reduce oxygen. The strong coupling in the GNR matrix between Co and oxygen ions increases the ionic nature of Co-O. As a result, Co^{3+} centres will serve as the additional NO_2 and electron adsorption centres indirectly removed from the p-type GNR through oxygen bridging, contributing to such an additional decrease in resistance in the presence of NO_2.

Another study on hybrid rGO with Co_3O_4 for NO_2 gas at room temperature was done by Zhang *et al.* (2018). The results indicated that the optimal hybrid exhibited a response of 26.8% to 5 ppm of NO_2 at room temperature, which was 2.27 times higher than that of undoped Co_3O_4 at 100°C. The hybrid sensor also showed fast response, excellent selectivity, long-term stability, and extremely low detection limit toward NO_2 at room temperature. The enhancement of sensing characteristics to NO_2 contributed to larger specific area, more chemisorbed oxygen species, and the hybridizing effect between Co_3O_4 and graphene in the hybrid [152].

Hybridizing Cu_2O and rGO-based sensor for enhancement of low concentration of NO_2 sensing at room temperature has been investigated by Pan *et al.* (2018). The

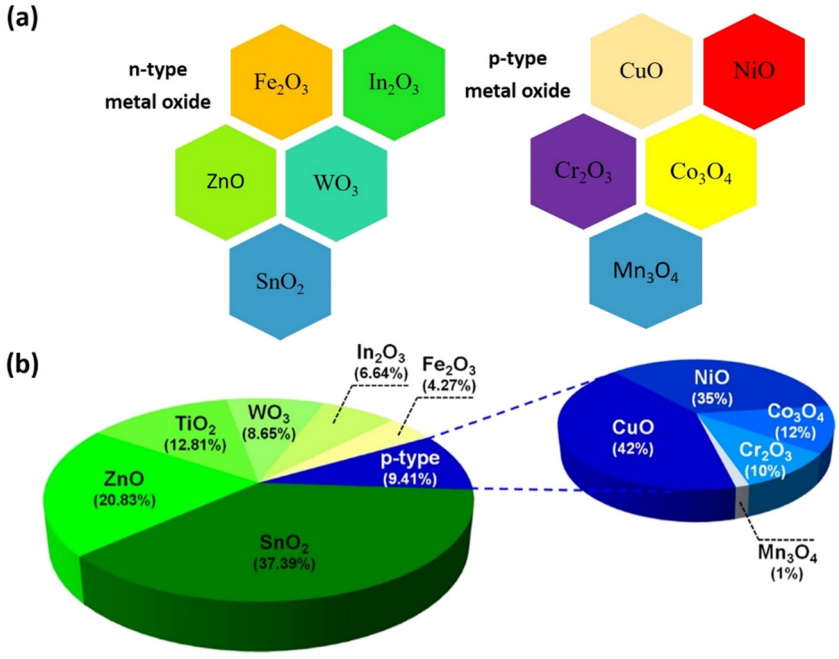

Figure 22: (a) Classification of n-type and p-type of metal oxide used as chemical sensor and (b) shows results of a search study on metal oxides semiconductor used as sensing materials for chemoresistive gas sensors. Reproduced from ref. [140].

sphere like of Cu_2O and the hybrids with rGO have been successfully synthesized by a facile solution-based self-assembly method. The gas sensing properties to 1 ppm of NO_2 at room temperature indicate that the 1 wt% of rGO/Cu_2O composite not only exhibits 2.8 times higher response than that of pristine Cu_2O and excellent selectivity, but also exhibit a rapid response and recovery at room temperature. The enhanced sensing characteristics mainly are attributed to increased gas adsorption active sites and the fast carriers transport due to the incorporating of rGO in the hybrid nanocomposites. Figure 23(a) shows FESEM images of GO nanocomposites and Cu_2O and Figure 23(b) shows response of sensor based on Cu_2O and 1 wt% rGO/Cu_2O to 1 ppm of different tested gases at room temperatures [153].

SnO_2 is one among the foremost promising inorganic n-type semiconductors with band gap of 3.62 eV at 298 K and exhibits excellent gas sensing properties having good response to varied sorts of toxic gases and organic vapours [154–158]. The hybrid rGO with SnO_2 nanomaterials-based gas sensors had obtained great attentions from the researchers [125,159–161]. Mao *et al.* (2012) had fabricated SnO_2 nano crystal incorporated with rGO sheet which was decorated onto Au IDEs, as a novel gas sensing device [125]. The sensors' manufactured performance demonstrated an optimum response to target gases at room temperature (detection limit 1 part per million (ppm) for NO_2) and a SnO_2 nanocrystal rGO strengthened the sensor signal to NO_2 but had weaken the sensor response to NH_3. Figure 24 shows comparison of gas sensing signals of NO_2 and NH_3 from pristine rGO sensors and rGO with SnO_2 nanocomposites.

Previous research by Zhang *et al.* (2014) has shown that the rGO/SnO_2 nanocomposites show an efficient sensing material for detection of NO_2 at temperature 50°C. The fabricated sensors shown in Figure 25(b) were by dropping the aqueous dispersion of products on a ceramic plate, which was previously coated with gold electrodes and ruthenium oxides as heater on frontal and back sides by screen printing technique followed by drying at room temperature. It is found that rGO/SnO_2 nanocomposites exhibit high response of 3.31 at 5 ppm NO_2, which is much higher than that of rGO (1.13), rapid response, and good selectivity and reproducibility. The enhanced gas sensing of the rGO/SnO_2 sensors was due to the formation of heterojunctions at the interface between SnO_2 and rGO and the effective electronic interaction between SnO_2 nanocrystals and rGO. This results in facilitating the detection of gases through the change in the electrical conductivity of the hybrid nanostructure. In addition, the binding of SnO_2 nanoparticles onto rGO contributes to more active sites (such as vacancies, defects, oxygen functional groups, and sp^2-bonded carbon) for the adsorption of NO_2 molecules; finally contributes to a higher sensitivity than pure rGO [160]. Figure 25(c) shows the sensing mechanism of the adsorption behaviour of NO_2

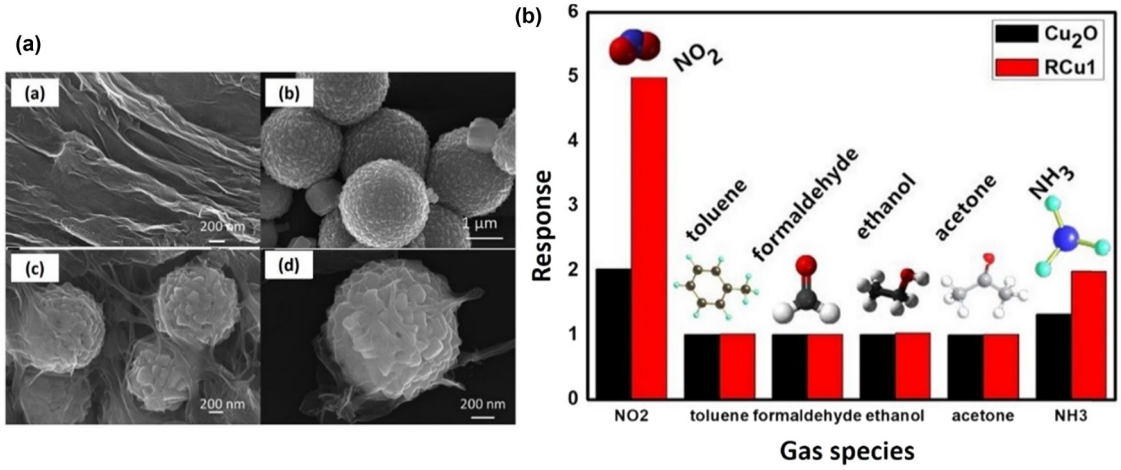

Figure 23: (a) FESEM images of (a) GO, (b) Cu_2O, and (c and d) 1 wt% of rGO/Cu_2O nanocomposite and (b) response of sensor based on Cu_2O and 1 wt% rGO/Cu_2O to 1 ppm of different tested gases at room temperatures. Reproduced from ref. [153].

molecules towards the rGO/SnO_2 nanocomposite proposed by Zhang *et al.* (2014).

For the sensing mechanism between the SnO_2 and rGO, the improvement of gas sensing performances on NO_2 sensor based on SnO_2–rGO-2 ($SnCl_4{\cdot}5H_2O$ added is 0.024 g) could be attributed to introduction of SnO_2 nanoparticles into the rGO matrix. This improvement also due to heterojunction has formed at the interface between SnO_2 and rGO. In open air, the first depletion layer is due to the adsorption of ionized oxygen (O_2^-) at the surface of the SnO_2 nanoparticles; the second is caused by the SnO_2–rGO heterojunction. Target gas molecules like NO_2 directly adsorb onto the surface of the SnO_2 nanoparticles and modify the depth of the first depletion layer, which in turn alters the depletion layer at the SnO_2–rGO interface. The effective electronic interaction between SnO_2 nanocrystals and the rGO facilitates the detection of gases through the change in the electrical conductivity of the hybrid nanostructure. The operation of chemical or gas sensors involves adsorption and desorption phenomena and reactions at the interface; the surface accessibility of nanocrystals is crucial to maintain their high response. As a result, hybrid SnO_2–rGO-2 system as a sensing element is potentially superior to either of its constituent components. rGOs coated with SnO_2 nanoparticles can detect gases that are normally undetectable by pristine rGOs. The attachment of SnO_2 nanoparticles onto rGOs leads to more active sites (such as vacancies, defects, oxygen functional groups as well as the sp^2-bonded carbon) for the adsorption of NO_2 molecules, and thus, a higher sensitivity than pure rGOs. Equations (4) and (5) show the reaction NO_2 molecules towards the rGO

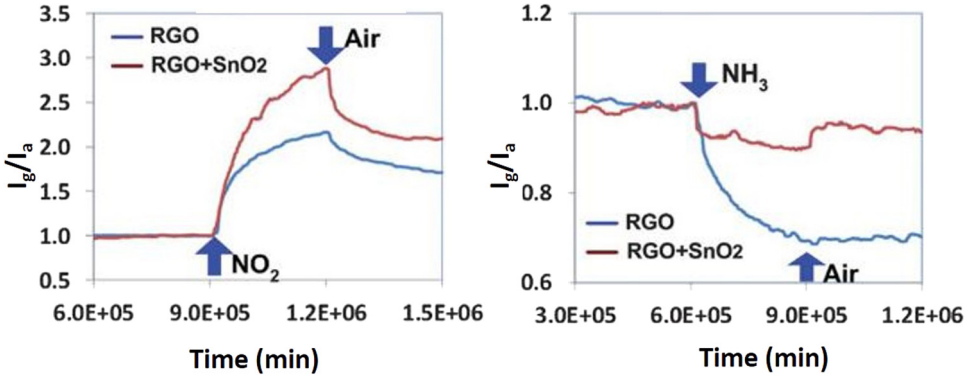

Figure 24: Gas sensing signals of NO_2 and NH_3 from pristine rGO sensors (blue line) and SnO_2 nanocomposites (red line). Reproduced from ref. [125].

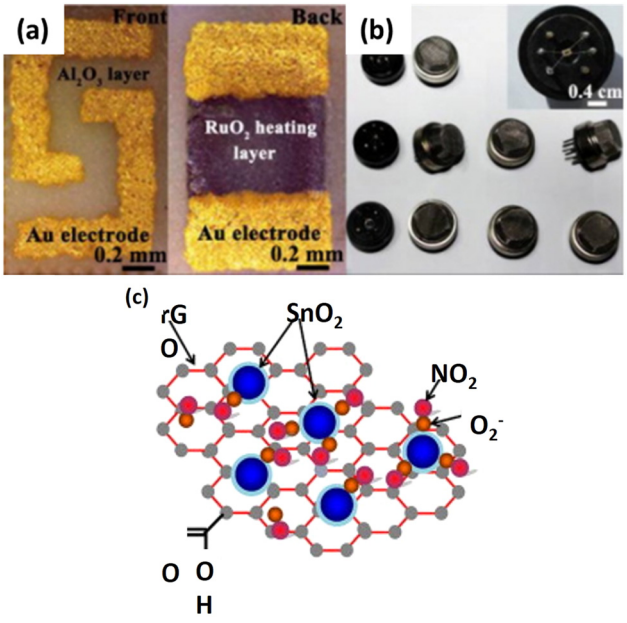

Figure 25: (a) Images of blank sensor used to detect NO_2 analytes, (b) images of the coated sensor with rGO/SnO_2 nanocomposites as sensing materials, and (c) as sensing mechanism on the adsorption behaviour of NO_2 molecules on the rGO/SnO_2 nanocomposite. Reproduced from ref. [160].

$$NO_2 + e^- \rightarrow NO_2^- \quad (4)$$

$$NO_2 + O_2^- \rightarrow NO^-O_2 \quad (5)$$

Cui *et al.* (2013) studies show indium (In) and ruthenium (Ru) doping in SnO_2 not only increases the sensing properties against NO_2, but also decreases the working temperature. Cui *et al.* (2013) had reported low-cost manufacturing hybrid nanomaterials in which In-doped SnO_2 (IDTO) nanoparticles, 2 to 3 nm in size, were uniformly distributed to rGO. The improved sensing efficiency of rGO/In-SnO_2 (rGO–IDTO) against NO_2 was demonstrated at room temperature hitting a detection limit as low as 0.3 ppm. In addition, excellent selectivity was also attained, as confirmed by other common gases tested such as NH_3, H_2, CO, and H_2S. Higher rGO–IDTO nanomaterials sensitivity indicates more NO_2 adsorption and more electron transfer from nanoparticles to NO_2. The higher sensitivity is also attributed by the improvement of higher surface-to-volume ratio of the nanoparticles exposed, which contributes to sufficient absorption sites in the sensing phase and thus increased sensitivity [161].

Another important n-type semiconductor, the WO_3, exhibits distinct physical and chemical properties, *viz.* has small band gap (about 2.585 eV) and stable physiochemical properties, which attracted considerable interest such as an active layer for chemical sensors [162,163]. An ultrafine rGO/WO_3 nanowire nanocomposite for highly sensitive toxic NH_3 gas sensors has been studied by Hung *et al.* (2020). The nanocomposites composed of single crystal WO_3 nanowires with an average size of 10 nm entangled by thin rGO layers. Sensing measurements confirmed that the rGO/WO_3 nanocomposite-based sensor can detect highly toxic NH_3 gas at low concentrations ranging from 20 to 500 ppm with detection limit of 138 ppb [164].

The development of rGO/WO_3 nanolamellae nanocomposites with different contents of rGO (0.5, 1, 2, 4 wt%) was synthesized *via* controlled hydrothermal method by Jiang *et al.* (2018) for acetylene (C_2H_2) gas detection at low operating temperature. Among four contents of prepared samples, sensing materials with 1 wt% rGO nanocomposite exhibited the best C_2H_2 sensing performance with lower optimal working temperature at 150°C, higher sensor response with 15.0 toward 50 ppm, faster response-recovery time at 52 and 27 s, lower detection limitation (1.3 ppm), long-term stability, and excellent repeatability. The enhancement of gas sensing performance of nanocomposite is possibly attributed to the formation of p–n heterojunction and the active interaction between WO_3 nanolamellae and rGO sheets. Besides, the introduction of rGO nanosheets leads to the impurity of synthesized materials, which creates more defects and promotes larger specific area for gas adsorption, outstanding conductivity, and faster carrier transport [165].

A room-temperature NO_2 gas sensor based on rGO/WO_3 nanocomposite films was fabricated using one-pot polyol process [166]. The sensor based on a nanocomposite film of rGO/WO_3 found that the introduction of rGO was effective for increasing the conductance of rGO/WO_3 nanocomposite film especially at strong response low concentration of NO_2 gas. When the amount of rGO added was below 3.2 wt%, the response (S) of the sensors dramatically increased and the concentration of NO_2 gas sensing increased with increasing the amount of rGO added. However, the amount of rGO added exceeded the percolation threshold, no variation in response versus concentration of NO_2 gas was clearly observed. The NO_2 gas sensor was very sensitive with acceptable linearity between 0.5 and 5 ppm, good reversibility, and long-term stability (at least 45 days) when used at room temperature.

Hydrothermally synthesized rGO/WO_3 nanocomposites-based gas sensor with interdigitated chromium electrode for NH_3 detection has been investigated by Punetha and Pandey (2019). The sensor shows the best performance at 150°C operating temperature; for 10 and 100 ppm of NH_3 gas concentration. The sensor response achieved 10.89

and 27.7 with 11/17 and 7/19 s response/recovery time, respectively. However, at room temperature, the sensor depicts the sensing response 4.35 with 13/20 s response/recovery time for 10 ppm of NH_3 gas concentration. The performance and stability of the device have been reported and analysed for different time intervals. This study paves a new approach to design and fabricate the gas sensing electronic device with high-performance parameters for semiconducting applications [167].

ZnO with a direct wide band gap (3.37 eV) and large exciton binding energy (60 meV) has been widely studied for gas sensing application due to its good response to a variety of reducing or oxidizing gases, low cost, and being friendly to the environment [168,169]. A highly sensitive room temperature of hydrogen gas sensor-based rGO/ZnO nanocomposites has been reported by Das *et al.* (2020). The ZnO nanoparticles were grown by chemical deposition method, while the rGO layer was produced by the electrochemical exfoliation using tetramethyle ammonium hydroxide (TMAH) as organic solvent and then drop-casted on the ZnO nanoparticles layer. The hybrid rGO–ZnO nanocomposite sensor with a Pd–Ag (70%) catalytic contact was tested for five different hydrogen concentrations (*e.g.* 100, 500, 1,000, 5,000, and 10,000 ppm) in synthetic air at room temperature. The sensor showed 484.1% response magnitude with 21.04 and 47.09 s response and recovery time at 100 ppm H_2, respectively [170].

Hierarchical rGO/ZnO hybrids with a flower-like morphology of ZnO and flexible rGO sheets were synthesized by a facile solution-processed method [171]. The gas sensing properties of hierarchical rGO/ZnO hybrids toward NO_2 were studied *via* a static system. The response of rGO/ZnO hybrids to 50 ppb NO_2 was 12, which was seven times higher than that of pristine ZnO at 100°C. The limit of detection achieved as low as 5 ppb. The enhanced sensor response was attributed to the presence of local p–n heterojunctions between rGO sheets and hierarchical structure of ZnO.

Referring to Das *et al.* (2020), an increased number of gas-interaction sites are probably directed to a high response magnitude of the sensor nanocomposites. The existence of band bending at the ZnO–rGO interface will accelerate more electron flow from ZnO to rGO. Additionally, high carrier mobility of rGO acted as an efficient cross-linkage among the neighbouring ZnO nanoparticles, resulting in faster response time. Besides that, the higher response magnitude is mainly due to the existence of more number of p–n heterojunction with additional oxygen adsorption site available at the rGO–ZnO interface. Such supportive hybridization of two prosperously sensing elements, ZnO nanoparticles and rGO, will aim at the creation of the next generation nanohybrid gas sensor devices with ever-increasing performance.

A sensitive and robust chemiresistive NO_2 gas sensing approach with the detection range of 5 ppb to 5 ppm using rGO/ZnO nanocomposite has been reported by Cao *et al.* (2020). It is investigated that the sensing response of rGO/ZnO sensor is significantly higher than ZnO sensor at 110°C working temperature. The rGO/ZnO sensor shows very low detection limit down to 5 ppb and high sensing bandwidth from 5 ppb to 5 ppm, indicating its potential use for gas sensing. The sensor exhibits high repeatability and long-term stability over the period. The sensitivity of NO_2 detection is due to large surface area and ultrahigh carrier mobility of rGO alongside high adsorption capability of ZnO nanospheres. This easily modulates depletion layer through fast electron transfer at the interface of heterojunction [172]. Figure 26(a) shows the schematic diagram for the synthesization of ZnO nanospheres by solvothermal method and the formation of rGO/ZnO heterostructure and Figure 26(b) shows the FESEM image of rGO/ZnO.

The MoO_3 nanoflakes coupled rGO with enhanced ethanol sensing performance and their mechanism has been investigated by Tang *et al.* (2019). The rGO/MoO_3 nanocomposites were fabricated through annealing process, and the rGO/MoO_3 shows high sensitivity, fast response, and good selectivity to ethanol. The response towards 100, 200, 500, and 8,000 ppm of ethanol is 53, 68.98, 117.0, and 702, respectively, which are 5.4, 4.83, 5.05, and 3.64 times higher than the MoO_3 at the working temperature of 310°C. In addition, the rGO/MoO_3 had shown good selectivity towards the ethanol over *n*-propanol, methanol, isopropanol, xylene, acetone, and benzene. Mo^{5+} also plays an important role in the sensing mechanism. The possible mechanism of the rGO/MoO_3 to ethanol is different from the traditional n-type semiconductors; both of the adsorbed oxygen and lattice oxygen participants in the reaction catalytically oxidize the ethanol into H_2O and CO_2 and result in the change of resistance. As a result, this indicates that the Mo^{5+} also plays an important role in the sensing process [173]. Figure 27 shows the schematic diagram of the sensing mechanism of rGO/MoO_3 to ethanol.

Bai *et al.* (2015) had used *in situ* microwave hydrothermal method in order to fabricate the heterojunction hybrids of rGO/α-MoO_3. With different rGO contents (2.5, 5, and 10 wt%), the sensing performance of 5 wt% of rGO/α-MoO_3 nanocomposites-based sensor to H_2S is significantly preferable. The nanocomposite demonstrates improved sensitivity, strong selectivity, rapid response, and recovery, as well as exhibits stability and repeatability

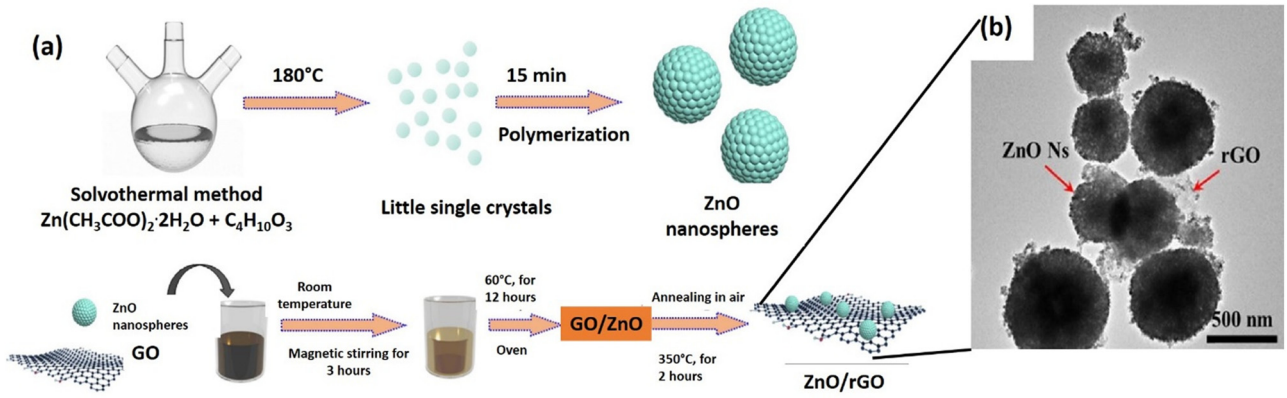

Figure 26: (a) schematic diagram for the synthesization of ZnO nanospheres by solvothermal method and the formation of rGO/ZnO heterostructure, and (b) rGO/ZnO image under FESEM at 500 nm. Reproduced from ref. [172].

in ppm-level H_2S at operating temperatures of 110°C, relative to those of pure MoO_3 as shown in Figure 28(a). The change in sensing efficiency can be due to the formation of heterojunction at the hybrid interface, which increases n-type surface area in MoO_3, thus promoting electron migration through the addition of rGO [174]. Figure 28(b) shows the response of 5 wt% of rGO/α-MoO_3 nanocomposites-based sensor towards different gases analysis at 100°C operating temperature.

Furthermore, referring to Bai *et al.* (2015), the improvement in sensing response could be attributed by these two factors: (1) the sensing response of semiconductor sensors involves adsorption and desorption phenomena and reactions at the interface; the surface accessibility of nanocrystals is crucial to maintain their high sensitivity. In particular, the 2D rGO sheets have created large 3D network architectures which enhance the interconnection of the MoO_3 and rGO. The rGO substrates are available in greater surface accessibility as well as rapid carrier transport to promote molecular adsorption, gas diffusion, and mass transport. (2) The enhancement of hybrid gas sensing can be due to electrons migrating at the interface between the MoO_3 nanorods and rGO nanosheets because of the disparity in their work function. In addition, the transfer of electrons at the interface further increases hybrid resistance in air because the depletion layer becomes thick. However, when the hybrid is subjected to reducing gas like H_2S, the H_2S will interact with oxygen ions absorbed onto the MoO_3 surface and releases the electrons to MoO_3, which results in a decrease in resistance [174].

Ye *et al.* (2016) had worked on rGO/TiO_2 layered film deposition on the interdigital electrode substrate *via* thermal treatment to trace detection of formaldehyde (CH_2O) at ambient temperature. The sensing performances of rGO/TiO_2 nanocomposites investigated over low detection concentrations from 0.1 to 0.5 ppmv revealed that the rGO/TiO_2 sensor exhibited rapid response, excellent selectivity, good reproducibility, and remarkable sensitivity of 0.8 ppm v^{-1},

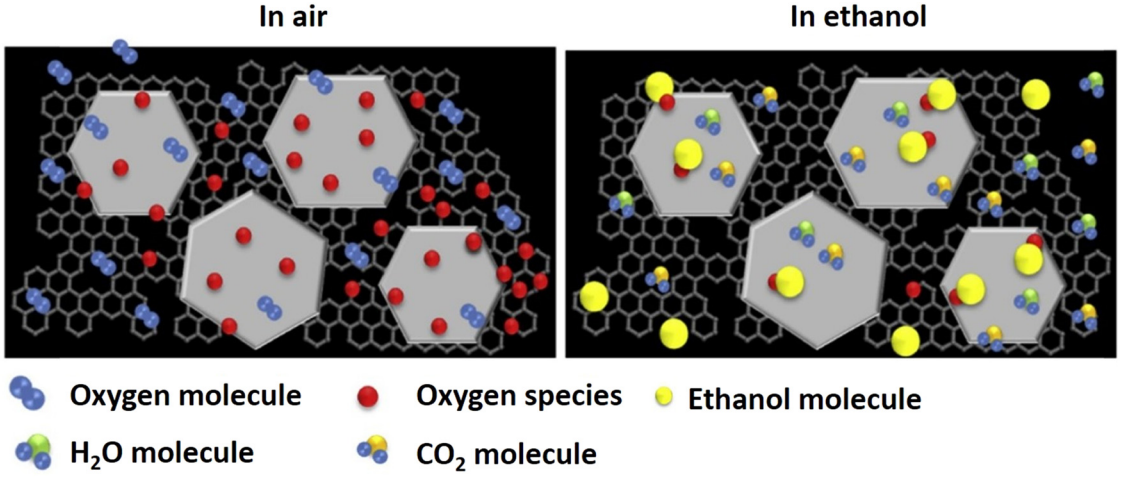

Figure 27: Schematic diagram of the sensing mechanism of rGO/MoO_3 to ethanol. Reproduced from ref. [173].

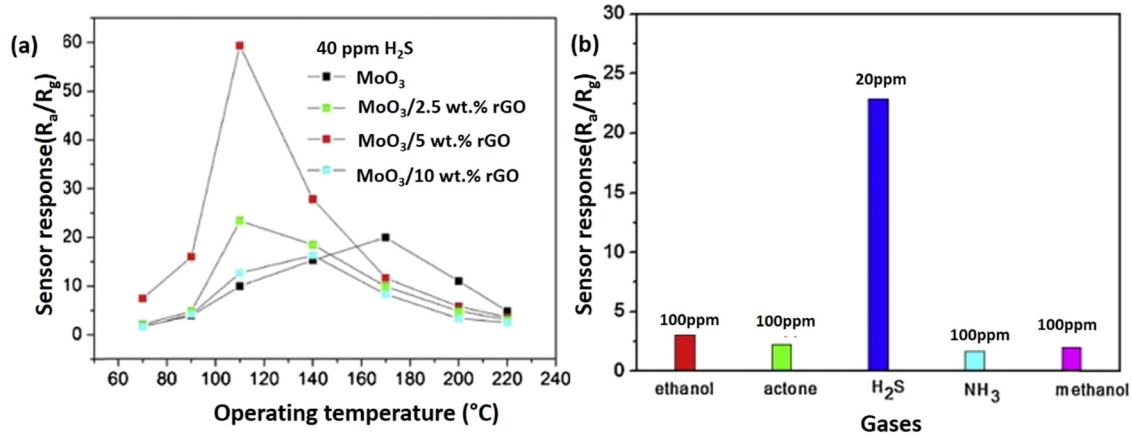

Figure 28: (a) Sensor response to 40 ppm of H_2S and (b) response of 5 wt% of rGO/α-MoO_3 nanocomposites-based sensor towards different gases analysis 100°C operating temperature. Reproduced from ref. [174].

which was higher than that of pristine rGO-based sensor (0.5 ppm v^{-1}) [175]. Another study on rGO/TiO_2 was done by Li *et al.* (2016) on the rGO-decorated TiO_2 microspheres nanocomposites-based chemiresistive-type sensor. The fabricated chemiresistive-type sensor using hydrothermal method shows good sensitivity and excellent selectivity to different concentrations of NH_3 from 5 to 50 ppm at room temperature. However, the response and recovery speeds of the sensor to NH_3 are slow and need further optimization [176]

The detection of NH_3 sensor working at room temperature has been successfully developed using rGO/TiO_2 [177]. rGO/TiO_2 hybrid through simple hydrothermal method and the sensor devices is easily fabricated through spray method to create conductive sensing network on the surface of IDEs. The sensing properties of the hybrid sensor suggest that introduction of TiO_2 into rGO significantly enhances the sensing performance. The main contributing factor for improved performance of rGO/TiO_2 hybrids in comparison to the pristine rGO is ascribed to the supporting function of TiO_2, which ameliorates the surface structure and enriches the active adsorption sites.

3.5 Performance of hybrid graphene/conductive polymer nanocomposites-based sensor

The development of highly sensitive and selective gas and vapour sensors based on graphene and their polymer nanocomposites has been attracted by the aforementioned properties. This section would address recent progress in the use of conductive polymer/graphene nanocomposites in sensors [178]. Many different types of organic materials have been used for gas sensing. The simplest organic compounds that can be electrically conductive are polymers, based on carbon and hydrogen [179]. Organic conductive polymers including PPy [180], polyaniline (PANI) [181], polythiophene (PTh) [182 and poly(3,4-ethylenedioxythiophene) (PEDOT) [183] are examples of materials for fabricating gas sensors. Some conducting polymers can behave like semiconductors due to their heterocyclic compounds which display physicochemical characteristics. As a result, reversible changes in the sensing layer's conductivity can be detected upon polar chemicals' adsorption on the surfaces at room temperature [184]. This effect is believed to be caused by the charge transfer between gas molecules and the polymer or swelling of the polymer films [118]. This sensing response has intensively increased motivation to develop high sensitive and selective chemical sensors by tailoring the compounds of different organic polymers with functionalized graphene.

Due to adsorption of interested chemical and gases, there are volumetric changes of the matrix polymer. This leads to a distinct change in percolation-type conductivity around a critical composition of the material, which is known as "percolation threshold". Generally, the percolation threshold is dependent on the shape of the conducting particle. Conductive polymer consisting of particles with higher aspect ratio shows lower threshold and higher sensitivity [185]. Consequently, by using conductive polymers, the sensitivity and selectivity of graphene-based chemical sensors can be enhanced. There have been numerous efforts in order to incorporate graphene or its derivatives with polymers.

Andre *et al.* (2017) had fabricated hybrid layer-by-layer (LbL) films of PANI/GO/ZnO gas sensors operating at room temperature which used to monitor the environment for hazardous pollutants like NH_3 gas. Because of synergistic effect in the materials properties, the films with 3 tetra layers were found to be the most adequate for detecting NH_3 in the range from 25 to 500 ppm with a response time of 30 s [186].

According to Huang *et al.* (2012), the hybrid rGO/PANI exhibited much rapid increase in resistance of 59.2% upon exposure to 50 ppm NH_3 gas as compared to a resistance change of about 5.2 and 13.4% for pristine rGO and pristine PANI nanofibre-based sensor, respectively. The rGO/PANI nanofibre hybrid sensitivity to NH_3 gas is 3.5 times higher than the sensitivity of pristine PANI nanofibre sensor and 10.4 times higher than the sensitivity of bare rGO. This much better sensitivity is due to the combined effect of rGO sheets and the decorated PANI nanoparticles. However, owing to the high surface ratio of rGO sheets and PANI nanoparticles, a long recovery time of 4 min for the sensing device based on rGO/PANI nanocomposites was observed. These hybrids have exhibited strong reversibility, long-term stable sensing efficiency under standard operating conditions, and high NH_3 gas selectivity in the presence of different analytes such as DMMP, methanol, dichloromethane, cyclohexane, and chloroform [187].

Li *et al.* (2018) studied about a sensitive sensor used for NH_3 detection at room temperature comprised of PANI nanosphere and GO-rambutan-PANIHs hybrids nanocomposites, with different weight percentages of GO (0.2–2 wt%). The nanocomposite was prepared by *in situ* chemical oxidative polymerization method and assembled on flexible polyethylene terephthalate (PET) substrate with no extra electrode. The efficiency of the gas sensor on the basis of 0.5 GO-rambutan-PANIHs nanocomposites shows the most sensitivity to the 10 ppm of NH_3 at room temperature. It exhibits response of approximately 31.8 for 100 ppm NH_3 and a rapid response time and recovery time of 102 and 186 s, respectively. This nanocomposite-based gas sensor achieved an amazing selectivity and an ultra-low detection limit of 50 ppb of NH_3 at room temperature [188]. Figure 29(a) and (b) shows the TEM image of rambutan-like PANIHs nanocomposites and Figure 29(c) the characteristic of the responses of sensors based on pure 0.2, 0.5, 1, and 2 wt% GO-PANIHs to 10 ppm NH_3 at room temperature.

A room temperature sub-ppb H_2S gas sensors based on SnO_2/rGO/PANI nanocomposites was synthesized by *in situ* polymerization technique by Zhang *et al.* [189]. The SnO_2/rGO/PANI nanocomposite film was manufactured using a polyethylene terephthalate (PET) substrate with interdigital electrodes (IDEs). The SnO_2/rGO/PANI sensor has excellent sensing characteristics such as high sensitivity, rapid response and recovery time, robust repeatability, excellent selectivity, and long-term stability. The response of the nanocomposite film sensor produced by *in situ* polymerization is 23.9 to 200 ppb H_2S, which is twice as high than that of physical doping method, and the detection limit is 50 ppb. The experimental result reveals that the SnO_2/rGO/PANI sensor is an excellent candidate to detect H_2S gas in exhaled human breath for early diagnosis of halitosis. The underlying sensing mechanism of the SnO_2/rGO/PANI sensing device towards H_2S gas is due to the high surface area of SnO_2/rGO/PANI film, chemisorption of oxygen on surface of SnO_2 hollow spheres, and the special role of heterojunction.

Xie *et al.* (2014) had reported the NO_2 detection behaviour of organic thin film transistor (OTFT)-based gas sensors employing pure P3HT film and rGO/P3HT bilayer films were compared. The results demonstrated an 80% improvement in the sensing response of OTFT gas sensor based on rGO/P3HT bilayer film which was due to the deposited rGO as the bottom layer of the bilayer film. The larger sensitivity of rGO/P3HT-based OTFT gas sensor is due to the peculiar properties of rGO such as large surface area due to 2D structure and availability of many graphitic carbon atoms as active sites for NO_2 adsorption. On exposure to other gases such as NH_3, SO_2, CO, CO_2, and H_2S, the sensing response of rGO/P3HT-based sensor was two orders of magnitude lower than that of NO_2, owing to the presence of P3HT layer that prevents the interference gases from contacting rGO. This work suggests that the low selectivity issue of graphene could get benefit from the functionalization of graphene with polymers [190].

Ye *et al.* (2014) have used rGO/P3HT nanocomposite films for fabricating NH_3 gas sensors and the rGO/P3HT films showed better sensitivity than rGO film sensor, where the sensor was prepared by the spray process. The improved sensor reaction has resulted from superior surface morphology in the composite films and the π–π interactions of the P3HT and rGO films. Sensitivity (7.15% for rGO/P3HT, 5.37% for rGO), reaction time (141 s for rGO/P3HT thin film, 637 s for rGO thin film), and recovery time (488 s for rGO/P3HT thin film; 609 s for rGO film) are all sensor parameters recorded [191].

Yang *et al.* (2014) had fabricated an efficient chemiresistive sensing platform using rGO-based nanocomposite with porous conductive polymer like PEDOT showed great promise for high performance gas sensing due to the enhanced sensitivity and selectivity of the gas sensor to NH_3

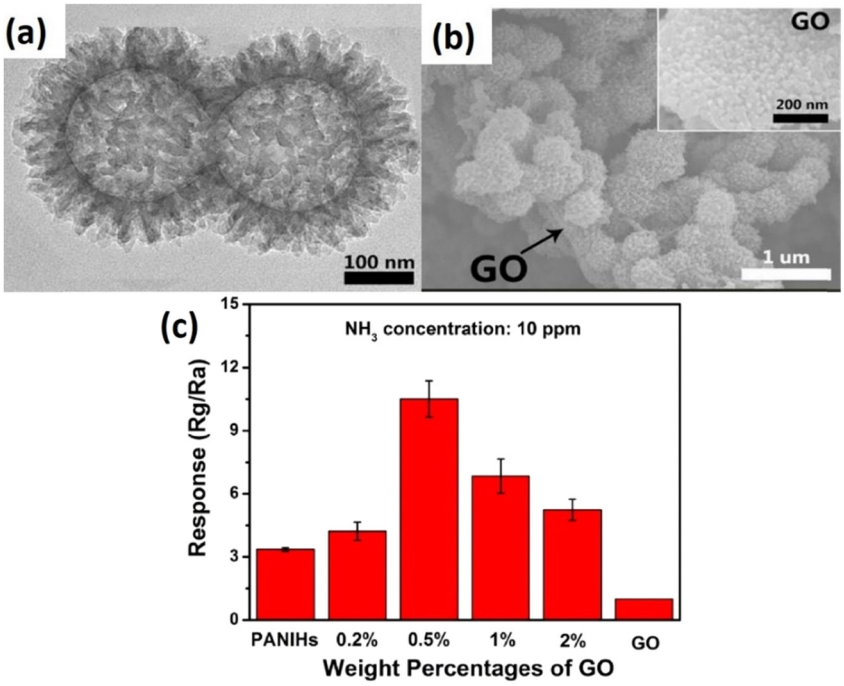

Figure 29: (a and b) TEM image of rambutan-like PANIHs and the nanocomposites, and (c) sensor response on the effect of weight percentages of GO. Reproduced from ref. [188].

gas at ppb-level. The gas sensing performance indicated that, in comparison to bare rGO and standard PEDOT, the porous rGO/PEDOT-based gas sensor displayed an apparent improvement in sensitivity and response/recovery performance (Figure 30). The vast area of the PEDOT and its open structure contributed to an excellent synergistic impact during the gas sensing phase between PEDOT and rGO. This nanocomposite-based sensor also demonstrated higher selectivity to NH_3 in comparison to other reduction analyte gases as a result of a uniform distribution of the PEDOT porous network in the rGO sheets [192].

A gas sensor device was developed using rGO-doped PEDOT-polystyrene sulfonate (PSS) organic thin film for the detection of NH_3 gas at room temperature [193]. The doping of rGO was used in PEDOT-PSS targeted to increase the conductivity of pristine PEDOT-PSS thin films by threefold. The gases such as NH_3, CO, NO_2, and nitrogen were used to test the sensing performance in the prepared thin films. The best gas sensitivity was achieved at 10 wt% of rGO-doped PEDOT-PSS thin film of about 87% for NH_3 gas with fast response and recovery times on exposing the sensor device to ammonia gas compared to other test gases such as CO, NO_2, and nitrogen. The sensor stability test shows the prepared sensor is highly stable even after a period of 1 month. Due to improved sensitivity, stability, and improved response and recovery times, these rGO-doped PEDOT-PSS organic thin films possibly will be used to detect NH_3 gas at low concentrations at room temperature.

The effect combination of PPy with 3D rGO to construct bioinspired nanocomposite for NH_3 sensing enhancement was conducted by Qin *et al.* (2019). The 3D-rGO, pre-prepared by a facile hydrothermal reduction method, serves as 3D skeleton to provide solid support for sensitive PPy nanoparticles attachment. The NH_3 sensing properties of the PPy/3D-rGO nanocomposite and the single components evaluated at room temperature found that the bioinspired PPy/3D-rGO nanocomposite displays a 4 to 5 times enhancement in gas response compared

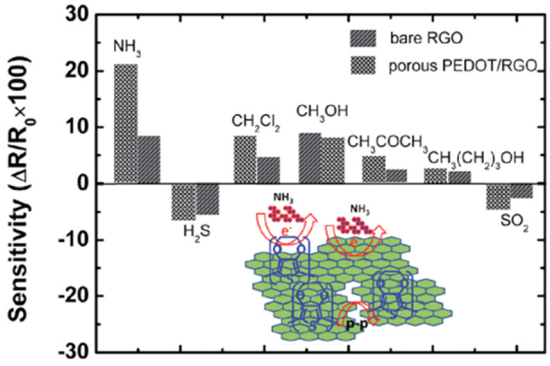

Figure 30: Gas selectivity of bare rGO and PEDOT/rGO-based sensing device towards 1 ppm various analyte gases. Reproduced from ref. [192].

Table 4: Summary of hybrid and non-hybrid graphene-based chemical sensor performance

Type of graphene	Metal oxide	Polymer	Chemical detection	Concentration	Sensor response	Response time	Recovery time	Reference
Graphene	Cu_2O	—	H_2S	5 ppb	11%	—	—	[196]
	Pd	PMMA	H_2	—	66.37%	1.8 min	5.5 min	[197]
	—	PANI	H_2	1 ppm	16.57%	2 min	3 min	[198]
	—	PANI	Toluene	100 ppm	35.5%	~11 min	54 min	[199]
	TiO_2	PPy	NH_3	50 ppm	36%	36 s	16 s	[200]
	—	PEDOT:PSS	NH_3	500 ppm	9.6%	3 min	5 min	[201]
	CuTsPc/N	PEDOT-PSS	NH_3	200 ppm	20%	2.5 min	1 min	[202]
Graphene quantum dots	S, N	PANI	NH_3	100 ppm	42.3%	1.92 min	0.73 min	[203]
	N	PANI	NH_3	1,500 ppm	110.92	7 min	0.083 min	[204]
GO	WO_3	—	NO_2	1 ppm	61	—	—	[205]
	ZnO	—	NH_3	1 ppm	24%	6 min	3 min	[206]
	ZnO	—	CO	22 ppm	24.3%	5 min	4 min	[206]
	ZnO	—	NO	5 ppm	−3.5%	25 min	—	[206]
	ZnO	PANI	NH_3	100 ppm	38.31%	30 s	—	[186]
	—	PANI	NH_3	100 ppm	11.33%	50 s	23 s	[207]
	TiO_2	PANI	NH_3	100 ppm	110%	32 s	17 s	[208]
	—	PANIH	NH_3	10 ppm	31.8	2 min	3 min	[188]
rGO	—	—	NO_2	100 ppm	1.41%	15 min	35 min	[209]
	—	—	NO_2	5 ppm	30%	>10 min	10 min	[210]
	Co_3O_4	—	NO_2	5 ppm	26.8%	1.5 min	40 min	[152]
	Co_3O_4	—	NO_2	60 ppm	80%	1 min	2 min	[149]
	Cu_2O	—	NO_2	2 ppm	67.8%	—	—	[145]
	SnO_2	—	NO_2	1 ppm	2.87	—	—	[125]
	SnO_2	—	NO_2	50 ppm	6.5%	3.17 min	3.73 min	[211]
	SnO_2	—	NO_2	8 ppm	~1,000%	5 min	8 min	[159]
	SnO_2	—	NO_2	5 ppm	3.31	2.25 min	3.33 min	[160]
	In-SnO_2	—	NO_2	100 ppm	11	11 min	—	[161]
	SnO_2	—	NO_2	1 ppm	700	11 min	6 min	[212]
	WO_3	—	NO_2	1 ppm	1.26	0.4–3 min	0.4–3 min	[213]
	WO_3	—	NO_2	56 ppm	40.8%	—	—	[214]
	Fe_3O_4	—	NO_2	400 ppm	24.2%	4.58 min	12.3 min	[215]
	—	P3HT (OTFT)	NO_2	2 ppm	7.5%	5 min	5 min	[190]
	ZnO	—	NO_2	50 ppm	8%	2.2 min	2.73 min	[216]
	ZnO	—	NO_2	5 ppm	119	2.3 min	4.3 min	[217]
	ZnO	—	CO	5 ppm	22.6	—	—	[217]
	ZnO	—	C_6H_6	5 ppm	19.1	—	—	[217]
	ZnO	—	C_2H_5OH	5 ppm	19.1	—	—	[217]
	Pd–WO_3	—	H_2	500 ppm	~10^2	<1 min	<1 min	[206]
	TiO_2	—	HCHO	1 ppmv	0.64	1 min	2 min	[175]
	TiO_2	—	NH_3	50 ppm	~5%	—	—	[176]
	—	—	NH_3	5 ppm	10%	>10 min	10 min	[210]
	—	P3HT	NH_3	10 ppm	7.15%	2 min	8 min	[191]
	—	PEDOT	NH_3	1 ppm	20%	1.5 min	2 min	[192]
	—	PANI	NH_3	50 ppm	59.2%	18 min	~4 min	[187]
	—	PANI	NH_3	50 ppm	47.6%	18 min	4 min	[218]
	—	PANI	NH_3	100 ppm	344.2	20 s	27 s	[219]
	SnO_2	PANI	NH_3	20 ppm	160%	13 min	30 min	[220]
	SnO_2	—	NH_3	1 ppm	1.12	—	—	[125]
	SnO_2	—	NH_3	50 ppm	15.9%	<1 min	<1 min	[221]
	SnO_2	PANI	H_2S	10 ppm	91.11%	—	—	[189]
	MoO_3	—	H_2S	20 ppm	23	9 s	17 s	[174]
	—	PANI	DMMP	50 ppm	22%	—	—	[218]
	Co_3O_4	—	Methanol	300 ppm	4%	4 min	6 min	[149]
	—	PEI	CO_2	1,000 ppm	0.7%	5 min	10 min	[222]

Table 4: Continued

Type of graphene	Metal oxide	Polymer	Chemical detection	Concentration	Sensor response	Response time	Recovery time	Reference
	Na-X	PPy	CO	1,000 ppm	77.4%	5.1 min	—	[223]
Graphene-carbon nanotubes	—	PMMA	Methane	10 ppm	0.55	—	—	[224]

with pure PPy or pure rGO and can rapidly respond to NH_3 with sub-ppm level. Pure PPy is known as a kind of sensing material operating at room temperature; the response values to 1 to 5 ppm of NH_3 are calculated to be 1.3 to 3.4. It is now proven that the response capability of PPy can be enhanced considerably after fabricated with 3D rGO. The enhanced sensing performances of PPy/3D-rGO nanocomposite are analysed reasonably based on its unique microstructure and the effective nanocompositeization between rGO and PPy nanoparticles [194].

For this reason, the ultrafast charge transfer occurring between the conjugated PPy and rGO can be explained by the π–π stacking that can also consequently promote the sensing performance of nanocomposite film. In other words, the strongly coupled hetero-interface between PPy and rGO due to vdW-bonded nanocompositeization endows the ultrafast charge transfer between each other and then also contributes to the enhanced sensing performance of the nanocomposite. Once the PPy/3D-rGO nanocomposite is exposed to NH_3, NH_3 molecules adsorb on the surface of the nanocomposite, and the H-bonding may take place between the adsorbed NH_3 and PPy or between NH_3 and rGO [93]. This could break the current H-bonding between rGO and PPy, encouraging an additional increase in resistance for PPy/3D-rGO nanocomposite sensor [195]. Table 4 shows the summary of hybrid and non-hybrid graphene-based chemical sensor performance towards their chemical detection.

4 Conclusions and future perspective

One of the nanocomposites applications highlighted is graphene-based chemical sensor. Graphene-based materials have been used as new sensing elements in developing gas and chemical sensors for wearable electronics due to their unique optical, electrical, mechanical, and thermal properties. The different types of sensors discussed here indicate that the right combination with doping materials, conductive polymer, and metal oxides device architectures, synergistically contributing interfacial effects, is important for high-performance of sensors. The detection performance of sensor is influenced by the chemical composition and structure, conductivity and charge transport surface area of morphological nanostructures, defects in graphene layered structures, functionalization sites, graphene interlayer spacing, concentration of analytes, intermolecular π–π interactions, along with its adsorption sites ability. At this stage, the parameters need to be considered for sensor are sensitivity, analyte concentration, operation temperature, limit of detection, recovery time, response time, response, and selectivity.

Further studies are paramount to discover each property and interaction on graphene-based nanocomposites. From the recent discoveries, chemical modifications of graphene would help to challenge the loops regarding its production, storage, handling, and processing as the modified graphene nanocomposites can have synergistic properties resulting from both graphene and the modifiers. Graphene nanocomposites can be tailored to have desired solubility and stability, tunable electrical, thermal and mechanical properties, and enhanced catalytic and biological properties. This can be achieved *via* either covalent or non-covalent chemical modifications of graphene. The former can be used to form graphene composites with strong affinity which finally will maximally keep the graphene's intrinsic properties. π–π stacking, hydrogen-bonding, van der Waals force, and coordination are the main interactions for non-covalent modifications. As a result, graphene nanocomposites modified *via* these methods, particularly generated *via* the π–π stacking process, would offer good mediums for any adaptable applications. In addition, through the chemical modification, either covalent bonding or non-covalent interactions can be realized. For the covalent modifications, it is usually achieved by a few techniques, such as atom doping or reaction with residual functional groups on graphene formed during the production or destruction of graphene's unsaturated structure, *via* destruction of conjugated structures, and modifications *via* residual structures.

In light of this, to be competitive with commercial sensors, graphene-based chemical sensor devices must be mass reproducible at low cost. Unlike CNTs, which do not exist in nature, graphene sheets are already present in graphite. It is worth to mention that GO is highly ranked functional substrate owing to its oxygen, which sometimes also leads to taking a part in the surface modification interactions and sometimes indirect detection of reactive gases. Therefore, top-down methods such as exfoliation of GO could be possible to be used for mass production graphene nanosheets at low cost. Such top-down techniques do not exist for most other categories of nanomaterials. Likewise, CVD synthesis of macro-GFs and roll-to-roll deposition of graphene on large area substrates by CVD could substantially lower the cost of graphene-based chemical sensors. These properties make them desired materials characteristics for the fabrication of intelligent and ultrasensitive sensors and green energy devices and competitive with commercial sensor technologies with mass production at low cost.

Acknowledgments: The authors would like to thank Department of Higher Education (JPT), Ministry of Higher Education Malaysia and The Science and Technology Facilities Council, United Kingdom (STFC), under Newton fund's Programand Malaysia Partnership and Alliances in Research (MyPAiR) for research grant ISIS-NEWTON/2019/SG/01 and Chemical Defence Research Centre (CHEMDEF), and National Defence University of Malaysia for a research grant UPNM/ 2018/CHEMDEFF/ST/3 are gratefully acknowledged.

Funding information: Newton fund's research grant ISIS-NEWTON/2019/SG/01 and Chemical Defence Research Centre (CHEMDEF) research grant UPNM/ 2018/CHEMDEFF/ST/3 are gratefully acknowledged.

Author contributions: All authors have accepted responsibility for the entire content of this manuscript and approved its submission.

Conflict of interest: The authors state no conflict of interest.

References

[1] Geim A, Novoselov K. The nobel prize in physics 2010. Sweden: Nobelprize org Nobel Media AB; 2010.

[2] Novoselov KS, Fal VI, Colombo L, Gellert PR, Schwab MG, Kim K. A roadmap for graphene. Nature. 2012;490(7419):192–200.

[3] Novoselov KS, Geim AK, Morozov SV, Jiang D, Zhang Y, Dubonos SV, et al. Electric field effect in atomically thin carbon films. Science. 2004;306(5696):666–9.

[4] Geim AK, Novoselov KS. The rise of graphene, in nanoscience and technology: a collection of reviews from nature journals. World Sci. 2010;11–9.

[5] Georgakilas V, Perman JA, Tucek J, Zboril R. Broad family of carbon nanoallotropes: classification, chemistry, and applications of fullerenes, carbon dots, nanotubes, graphene, nanodiamonds, and combined superstructures. Chem Rev. 2015;115(11):4744–822.

[6] Allen MJ, Tung VC, Kaner RB. Honeycomb carbon: a review of graphene. Chem Rev. 2010;110(1):132–45.

[7] Chandrasekar M, Senthil MKT, Senthilkumar K, Mohd Nurazzi N, Sanjay MR, Rajini N, et al. Inorganic. Nanofillers-based thermoplastic and thermosetting composites. Lightweight polymer composite structures. CRC Press; 2020. p. 309–30.

[8] Liu C, Huang X, Wu YY, Deng X, Liu J, Zheng Z, et al. Review on the research progress of cement-based and geopolymer materials modified by graphene and graphene oxide. Nanotechnol Rev. 2020;9(1):155–69.

[9] Sang M, Shin J, Kim K, Yu KJ. Electronic and thermal properties of graphene and recent advances in graphene based electronics applications. Nanomater. 2019;9(3):374.

[10] Novoselov KS, Geim AK, Morozov SV, Jiang D, Katsnelson MI, Grigorieva I, et al. Two-dimensional gas of massless Dirac fermions in graphene. Nature. 2005;438(7065):197–200.

[11] Zhang Y, Tan YW, Stormer HL, Kim P. Experimental observation of the quantum Hall effect and Berry's phase in graphene. Nature. 2005;438(7065):201–4.

[12] Fathi D. A review of electronic band structure of graphene and carbon nanotubes using tight binding. J Nanotechnol. 2011;1–6.

[13] Yavari F, Koratkar N. Graphene-based chemical sensors. J Phys Chem Lett. 2012;3(13):1746–53.

[14] Collins PG, Bradley K, Ishigami M, Zettl DA. Extreme oxygen sensitivity of electronic properties of carbon nanotubes. Science. 2000;287(5459):1801–4.

[15] Kong J, Franklin NR, Zhou C, Chapline MG, Peng S, Cho K, et al. Nanotube molecular wires as chemical sensors. Science. 2000;287(5453):622–5.

[16] Modi A, Koratkar N, Lass E, Wei B, Ajayan PM. Miniaturized gas ionization sensors using carbon nanotubes. Nature. 2003;424(6945):171–4.

[17] Schedin F, Geim AK, Morozov SV, Hill EW, Blake P, Katsnelson MI, et al. Detection of individual gas molecules adsorbed on graphene. Nat Mater. 2007;6(9):652–5.

[18] Cao Y, Fatemi V, Demir A, Fang S, Tomarken SL, Luo JY, et al. Correlated insulator behaviour at half-filling in magic-angle graphene superlattices. Nature. 2018;556(7699):80–4.

[19] Cao Y, Fatemi V, Fang S, Watanabe K, Taniguchi T, Kaxiras E, et al. Unconventional superconductivity in magic-angle graphene superlattices. Nature. 2018;556(7699):43–50.

[20] Ichinokura S, Sugawara K, Takayama A, Takahashi T, Hasegawa S. Superconducting calcium-intercalated bilayer graphene. ACS Nano. 2016;10(2):2761–5.
[21] Gibney E. Surprise graphene discovery could unlock secrets of superconductivity. Nature. 2018;555:151–2.
[22] Mele EJ. Novel electronic states seen in graphene. Nature. 2018;556:37–8.
[23] Hernaez M, Zamarreño CR, Melendi-Espina S, Bird LR, Mayes AG, Arregui FJ. Optical fibre sensors using graphene-based materials: a review. Sensors. 2017;17(1):1–24.
[24] Bai RG, Muthoosamy K, Manickam S, Hilal-Alnaqbi A. Graphene-based 3D scaffolds in tissue engineering: fabrication, applications, and future scope in liver tissue engineering. Int J Nanomed. 2019;14:5753–83.
[25] Qureshi TS, Panesar DK. A comparison of graphene oxide, reduced graphene oxide and pure graphene: early age properties of cement composites. 2nd RILEM Spring Convention & International Conference on Sustainable Materials, Systems and Structures. Rovinj, Croatia: 2019.
[26] Chuah S, Pan Z, Sanjayan JG, Wang CM, Duan WH. Nano reinforced cement and concrete composites and new perspective from graphene oxide. Constr Build Mater. 2014;73:113–24.
[27] Lv W, Li Z, Deng Y, Yang QH, Kang F. Graphene-based materials for electrochemical energy storage devices: opportunities and challenges. Energy Storage Mater. 2016;2:107–38.
[28] Zhu Y, Murali S, Cai W, Li X, Suk JW, Potts JR, et al. Graphene and graphene oxide: synthesis, properties, and applications. Adv Mater. 2010;22(35):3906–24.
[29] Compton OC, Nguyen ST. Graphene oxide, highly reduced graphene oxide, and graphene: versatile building blocks for carbon-based materials. Small. 2010;6(6):711–23.
[30] Wan S, Chen Y, Wang Y, Li G, Wang G, Liu L, et al. Ultrastrong graphene films *via* long-chain π-bridging. Matter. 2019;1(2):389–401.
[31] Bonaccorso F, Lombardo A, Hasan T, Sun Z, Colombo L, Ferrari AC. Production and processing of graphene and 2d crystals. Mater Today. 2012;15(12):564–89.
[32] Krishnamoorthy K, Veerapandian M, Yun K, Kim SJ. The chemical and structural analysis of graphene oxide with different degrees of oxidation. Carbon. 2013;53:38–49.
[33] Stankovich S, Dikin DA, Piner RD, Kohlhaas KA, Kleinhammes A, Jia Y, et al. Synthesis of graphene-based nanosheets *via* chemical reduction of exfoliated graphite oxide. Carbon. 2007;45(7):1558–65.
[34] Kazi SN, Badarudin A, Zubir MN, Ming HN, Misran M, Sadeghinezhad E, et al. Investigation on the use of graphene oxide as novel surfactant to stabilize weakly charged graphene nanoplatelets. Nanoscale Res Lett. 2015;10(1):1–15.
[35] Sharma N, Sharma V, Jain Y, Kumari M, Gupta R, Sharma SK, et al. Synthesis and characterization of graphene oxide (GO) and reduced graphene oxide (rGO) for gas sensing application. Macromolecular Symposia. Germany: Wiley Online Library; 2017.
[36] Yang H, Zhou W, Yu B, Wang Y, Cong C, Yu T. Uniform decoration of reduced graphene oxide sheets with gold nanoparticles. J Nanotechnol. 2012;2012:328565.
[37] Schrier J. Fluorinated and nanoporous graphene materials as sorbents for gas separations. ACS Appl Mater Interfaces. 2011;3(11):4451–8.
[38] Inagaki M, Kang F. Graphene derivatives: graphane, fluorographene, graphene oxide, graphyne and graphdiyne. J Mater Chem A. 2014;2(33):13193–206.
[39] Dey A. Semiconductor metal oxide gas sensors: a review. Mater Sci Eng B. 2018;229:206–17.
[40] Rzaij JM, Abass AM. Review on: TiO_2 thin film as a metal oxide gas sensor. Chem Rev. 2020;2(2):114–21.
[41] Tyagi P, Sharma A, Tomar M, Gupta V. Metal oxide catalyst assisted SnO_2 thin film based SO_2 gas sensor. Sens Actuators B Chem. 2016;224:282–9.
[42] Shendage SS, Patil VL, Vanalakar SA, Patil SP, Harale NS, Bhosale JL, et al. Sensitive and selective NO_2 gas sensor based on WO_3 nanoplates. Sens Actuators B Chem. 2017;240:426–33.
[43] Ponzoni A, Baratto C, Cattabiani N, Falasconi M, Galstyan V, Nunez-Carmona E, et al. Metal oxide gas sensors, a survey of selectivity issues addressed at the SENSOR Lab, Brescia (Italy). Sensors. 2017;17(4):1–27.
[44] Demon SZ, Kamisan AI, Abdullah N, Noor SA, Khim OK, Kasim NA, et al. Graphene-based materials in gas sensor applications: a review. Sens Mater. 2020;32:759–77.
[45] Liu X, Cheng S, Liu H, Hu S, Zhang D, Ning H. A survey on gas sensing technology. Sensors. 2012;12(7):9635–65.
[46] Nurazzi NM, Harussani MM, Zulaikha NS, Norhana AH, Syakir MI, Norli A. Composites based on conductive polymer with carbon nanotubes in DMMP gas sensors–an overview. Polimery. 2021;66(2):85–97.
[47] Vilanova X. Special issue "Advanced nanomaterials based gas sensors". Sensors. 2020;20(5):1–5.
[48] Norizan MN, Moklis MH, Demon SZ, Halim NA, Samsuri A, Mohamad IS, et al. Carbon nanotubes: functionalisation and their application in chemical sensors. RSC Adv. 2020;10(71):43704–32.
[49] Chatterjee SG, Chatterjee S, Ray AK, Chakraborty AK. Graphene–metal oxide nanohybrids for toxic gas sensor: a review. Sens Actuators B Chem. 2015;221:1170–81.
[50] Mondal TK, Dinda D, Saha SK. Nitrogen, sulphur co-doped graphene quantum dot: an excellent sensor for nitroexplosives. Sens Actuators B Chem. 2018;257:586–93.
[51] Tung TT, Tran MT, Feller JF, Castro M, Van Ngo T, Hassan K, et al. Graphene and metal organic frameworks (MOFs) hybridization for tunable chemoresistive sensors for detection of volatile organic compounds (VOCs) biomarkers. Carbon. 2020;159:333–44.
[52] Bottari G, Herranz MÁ, Wibmer L, Volland M, Rodríguez-Pérez L, Guldi DM, et al. Chemical functionalization and characterization of graphene-based materials. Chem Soc Rev. 2017;46(15):4464–500.
[53] Jiang L, Fan Z. Design of advanced porous graphene materials: from graphene nanomesh to 3D architectures. Nanoscale. 2014;6(4):1922–45.
[54] Rajesh GZ, Charlie Johnson AT, Puri N, Mulchandani A, Aswal DK. Scalable chemical vapor deposited graphene field-effect transistors for bio/chemical assay. Appl Phys Rev. 2021;8(1):011311.
[55] Yun YJ, Hong WG, Choi NJ, Park HJ, Moon SE, Kim BH, et al. A 3D scaffold for ultra-sensitive reduced graphene oxide gas sensors. Nanoscale. 2014;6(12):6511–4.
[56] Mishra SK, Tripathi SN, Choudhary V, Gupta BD. SPR based fibre optic ammonia gas sensor utilizing nanocomposite

film of PMMA/reduced graphene oxide prepared by *in situ* polymerization. Sens Actuators B Chem. 2014;199:190–200.
[57] Lin YM, Avouris P. Strong suppression of electrical noise in bilayer graphene nanodevices. Nano Lett. 2008;8(8):2119–25.
[58] Hill EW, Vijayaragahvan A, Novoselov K. Graphene sensors. IEEE Sens J. 2011;11(12):3161–70.
[59] Booth TJ, Blake P, Nair RR, Jiang D, Hill EW, Bangert U, et al. Macroscopic graphene membranes and their extraordinary stiffness. Nano Lett. 2008;8(8):2442–6.
[60] Li W, Geng X, Guo Y, Rong J, Gong Y, Wu L, et al. Reduced graphene oxide electrically contacted graphene sensor for highly sensitive nitric oxide detection. ACS Nano. 2011;5(9):6955–61.
[61] Chung MG, Lee HM, Kim T, Choi JH, Kyun Seo D, Yoo JB, et al. Highly sensitive NO_2 gas sensor based on ozone treated graphene. Sens Actuators B Chem. 2012;166:172–6.
[62] Kulkarni GS, Reddy K, Zhong Z, Fan X. Graphene nanoelectronic heterodyne sensor for rapid and sensitive vapour detection. Nat Commun. 2014;5(1):1–7.
[63] Alahi ME, Nag A, Mukhopadhyay SC, Burkitt L. A temperature-compensated graphene sensor for nitrate monitoring in real-time application. Sens Actuator A Phys. 2018;269:79–90.
[64] Ratinac KR, Yang W, Ringer SP, Braet F. Toward ubiquitous environmental gas sensors-capitalizing on the promise of graphene. Env Sci Technol. 2010;44(4):1167–76.
[65] Segal M. Selling graphene by the ton. Nat Nanotechnol. 2009;4(10):612–4.
[66] Mohd Nurazzi N, Muhammad Asyraf MR, Khalina A, Abdullah N, Sabaruddin FA, Kamarudin SH, et al. Fabrication, functionalization, and application of carbon nanotube-reinforced polymer composite: an overview. Polymers. 2021;13(7):1047.
[67] Lu G, Yu K, Ocola LE, Chen J. Ultrafast room temperature NH_3 sensing with positively gated reduced graphene oxide field-effect transistors. Chem Commun. 2011;47(27):7761–3.
[68] Gutés A, Hsia B, Sussman A, Mickelson W, Zettl A, Carraro C, et al. Graphene decoration with metal nanoparticles: towards easy integration for sensing applications. Nanoscale. 2012;4(2):438–40.
[69] Niu F, Liu JM, Tao LM, Wang W, Song WG. Nitrogen and silica co-doped graphene nanosheets for NO_2 gas sensing. J Mater Chem A. 2013;1(20):6130–3.
[70] Russo PA, Donato N, Leonardi SG, Baek S, Conte DE, Neri G, et al. Room-temperature hydrogen sensing with heterona-nostructures based on reduced graphene oxide and tin oxide. Angew Chem Int Ed. 2012;51(44):11053–57.
[71] Paul RK, Badhulika S, Saucedo NM, Mulchandani A. Graphene nanomesh as highly sensitive chemiresistor gas sensor. Anal Chem. 2012;84(19):8171–8.
[72] Tiwari SK, Sahoo S, Wang N, Huczko A. Graphene research and their outputs: status and prospect. J Sci Adv Mater Dev. 2020;5(1):10–29.
[73] Mao S, Yu K, Cui S, Bo Z, Lu G, Chen J. A new reducing agent to prepare single-layer, high-quality reduced graphene oxide for device applications. Nanoscale. 2011;3(7):2849–53.
[74] Yang W, Mao S, Yang J, Shang T, Song H, Mabon J, et al. Large-deformation and high-strength amorphous porous carbon nanospheres. Sci Rep. 2016;6(1):1–9.
[75] Alemour B, Yaacob MH, Lim HN, Hassan MR. Review of electrical properties of graphene conductive composites. Int J Nanoelectron Mater. 2018;11(4):371–98.
[76] AZoM. Graphite (C) – Classifications, properties & applications. United Kingdom; 2002; Available from: https://www.azom.com
[77] Castañeda LF, Walsh FC, Nava JL, de León CP. Graphite felt as a versatile electrode material: properties, reaction environment, performance and applications. Electrochim Acta. 2017;258:1115–39.
[78] Spahr ME, Zürcher S, Rodlert-bacilieri M, Mornaghini F, Gruenberger TM, Imertech SAS. High-conductive carbon black with low viscosity. United States patent US 10870761; 2020 Dec 22.
[79] Lu W, He T, Xu B, He X, Adidharma H, Radosz M, et al. Progress in catalytic synthesis of advanced carbon nanofibers. J Mater Chem A. 2017;5(27):13863–81.
[80] David B, Patrick P, Andrew P. Carbon nanofiber applications & properties. Germany; 2020; Available from: https://www.sigmaaldrich.com
[81] Kavitha M, Kalpana AM. Carbon nanotubes: properties and applications-A brief review. i-manager's J ElectrEng. 2017;7(3):1–6.
[82] Spinelle L, Gerboles M, Kok G, Persijn S, Sauerwald T. Review of portable and low-cost sensors for the ambient air monitoring of benzene and other volatile organic compounds. Sensors. 2017;17(7):1–30.
[83] Norizan MN, Zulaikha NS, Norhana AB, Syakir MI, Norli A. Carbon nanotubes-based sensor for ammonia gas detection–an overview. Polimery. 2021;66(3):175–86.
[84] Giddey SP, Badwal SP, Kulkarni A. Review of electrochemical ammonia production technologies and materials. Int J Hydrog Energy. 2013;38(34):14576–94.
[85] Miller DR, Akbar SA, Morris PA. Nanoscale metal oxide-based heterojunctions for gas sensing: a review. Sens Actuators B Chem. 2014;204:250–72.
[86] Ahuja T, Kumar D. Recent progress in the development of nano-structured conducting polymers/nanocomposites for sensor applications. Sens Actuators B Chem. 2009;136(1):275–86.
[87] Baharuddin AA, Ang BC, Haseeb AS, Wong YC, Wong YH. Advances in chemiresistive sensors for acetone gas detection. Mater Sci Semicond Process. 2019;103:1–19.
[88] Hou L, Zhang C, Li L, Du C, Li X, Kang XF, et al. CO gas sensors based on p-type CuO nanotubes and CuO nanocubes: morphology and surface structure effects on the sensing performance. Talanta. 2018;188:41–9.
[89] Jaisutti R, Lee M, Kim J, Choi S, Ha TJ, Kim J, et al. Ultrasensitive room-temperature operable gas sensors using p-type Na: ZnO nanoflowers for diabetes detection. ACS Appl Mater Interfaces. 2017;9(10):8796–804.
[90] Tian W, Liu X, Yu W. Research progress of gas sensor based on graphene and its derivatives: a review. Appl Sci. 2018;8(7):1–21.
[91] Jawaid M, Ahmad A, Lokhat D. Graphene-based nanotechnologies for energy and environmental applications. Netherlands: Elsevier; 2019.
[92] Jeevitha G, Abhinayaa R, Mangalaraj D, Ponpandian N, Meena P, Mounasamy V, et al. Porous reduced graphene oxide (rGO)/WO_3 nanocomposites for the enhanced

detection of NH_3 at room temperature. Nanoscale Adv. 2019;1(5):1799–811.
[93] Joshi A, Gangal SA, Gupta SK. Ammonia sensing properties of polypyrrole thin films at room temperature. Sens Actuators B Chem. 2011;156(2):938–42.
[94] Leenaerts O, Partoens B, Peeters FM. Adsorption of H_2O, NH_3, CO, NO_2, and NO on graphene: a first-principles study. Phys Rev B. 2008;77(12):1–6.
[95] Tang X, Raskin JP, Kryvutsa N, Hermans S, Slobodian O, Nazarov AN, et al. An ammonia sensor composed of polypyrrole synthesized on reduced graphene oxide by electropolymerization. Sens Actuators B Chem. 2020;305:1–10.
[96] Yavari F, Chen Z, Thomas AV, Ren W, Cheng HM, Koratkar N. High sensitivity gas detection using a macroscopic three-dimensional graphene foam network. Sci Rep. 2011;1(1):1–5.
[97] Gerasimov G, Pogosbekian M. Graphene-based gas sensors. in Advanced environmental analysis, United Kingdom; 2016. p. 133–52.
[98] Capone S, Forleo A, Francioso L, Rella R, Siciliano P, Spadavecchia J, et al. Solid state gas sensors: state of the art and future activities. J Optoelectron Adv Mater. 2003;5(5):1335–48.
[99] Bak SY, Lee J, Kim Y, Lee SH, Woo K, Lee S, et al. Sensitivity improvement of urchin-like ZnO nanostructures using 2wo-dimensional electron gas in MgZnO/ZnO. Sensors. 2019;19(23):5195.
[100] Tyagi D, Wang H, Huang W, Hu L, Tang Y, Guo Z, et al. Recent advances in two-dimensional-material-based sensing technology toward health and environmental monitoring applications. Nanoscale. 2020;12(6):3535–59.
[101] Chu BH, Lo CF, Nicolosi J, Chang CY, Chen V, Strupinski W, et al. Hydrogen detection using platinum coated graphene grown on SiC. Sens Actuators B Chem. 2011;157(2):500–3.
[102] Chen CW, Hung SC, Yang MD, Yeh CW, Wu CH, Chi GC, et al. Oxygen sensors made by monolayer graphene under room temperature. Appl Phys Lett. 2011;99(24):1–3.
[103] Zhang S, Zhou J, Wang Q, Chen X, Kawazoe Y, Jena P. Penta-graphene: a new carbon allotrope. Proceedings of the National Academy of Sciences; 2015.
[104] Cheng MQ, Chen Q, Yang K, Huang WQ, Hu WY, Huang GF. Penta-graphene as a potential gas sensor for NO_x detection. Nanoscale Res Lett. 2019;14(1):1–8.
[105] Lee G, Yang G, Cho A, Han JW, Kim J. Defect-engineered graphene chemical sensors with ultrahigh sensitivity. Phys Chem Chem Phys. 2016;18(21):14198–204.
[106] Kumar S, Kaushik S, Pratap R, Raghavan S. Graphene on paper: a simple, low-cost chemical sensing platform. ACS Appl Mater Interfaces. 2015;7(4):2189–94.
[107] Seekaew Y, Phokharatkul D, Wisitsoraat A, Wongchoosuk C. Highly sensitive and selective room-temperature NO_2 gas sensor based on bilayer transferred chemical vapor deposited graphene. Appl Surf Sci. 2017;404:357–63.
[108] Jeong SY, Jeong S, Lee SW, Kim ST, Kim D, Jeong HJ, et al. Enhanced response and sensitivity of self-corrugated graphene sensors with anisotropic charge distribution. Sci Rep. 2015;5(1):1–9.
[109] Ruffino F, Meli G, Grimaldi MG. Nanoscale electrical characteristics of metal (Au, Pd)–graphene–metal (Cu) contacts. Solid State Commun. 2016;225:1–6.
[110] Khan ZU, Kausar A, Ullah H, Badshah A, Khan WU. A review of graphene oxide, graphene buckypaper, and polymer/graphene composites: properties and fabrication techniques. J Plast Film Sheeting. 2016;32(4):336–79.
[111] Choi YR, Yoon YG, Choi KS, Kang JH, Shim YS, Kim YH, et al. Role of oxygen functional groups in graphene oxide for reversible room-temperature NO_2 sensing. Carbon. 2015;91:178–87.
[112] Jang HW, Shim YS, Kim YH. Heaterless operation of chemoresistive gas sensors for further functional convergence. Smart sensors for health and environment monitoring. Germany: Springer; 2015. p. 189–212
[113] Peng Y, Li J. Ammonia adsorption on graphene and graphene oxide: a first-principles study. Front Env Sci Eng. 2013;7(3):403–11.
[114] Varghese SS, Lonkar S, Singh KK, Swaminathan S, Abdala A. Recent advances in graphene based gas sensors. Sens Actuators B Chem. 2015;218:160–83.
[115] Mattson EC, Pande K, Unger M, Cui S, Lu G, Gajdardziska-Josifovska M, et al. Exploring adsorption and reactivity of NH_3 on reduced graphene oxide. J Phys Chem C. 2013;117(20):10698–707.
[116] Alam MK, Rahman MM, Rahman MM, Kim D, Asiri AM, Khan FA. *In-situ* synthesis of gold nanocrystals anchored graphene oxide and its application in biosensor and chemical sensor. J Electroanal Chem. 2019;835:329–37.
[117] Yu C, Wu Y, Liu X, Fu F, Gong Y, Rao YJ, et al. Miniature fiber-optic NH_3 gas sensor based on Pt nanoparticle-incorporated graphene oxide. Sens Actuators B Chem. 2017;244:107–13.
[118] Hunter GW, Akbar S, Bhansali S, Daniele M, Erb PD, Johnson K, et al. Editors' choice – critical review – a critical review of solid state gas sensors. J Electrochem Soc. 2020;167(3):1–30.
[119] Park MS, Kim KH, Kim MJ, Lee YS. NH_3 gas sensing properties of a gas sensor based on fluorinated graphene oxide. Colloids Surf A Physicochem Eng Asp. 2016;490:104–9.
[120] Prezioso S, Perrozzi F, Giancaterini L, Cantalini C, Treossi E, Palermo V, et al. Graphene oxide as a practical solution to high sensitivity gas sensing. J Phys Chem C. 2013;117(20):10683–90.
[121] Wang J, Singh B, Park JH, Rathi S, Lee IY, Maeng S, et al. Dielectrophoresis of graphene oxide nanostructures for hydrogen gas sensor at room temperature. Sens Actuators B Chem. 2014;194:296–302.
[122] Some S, Xu Y, Kim Y, Yoon Y, Qin H, Kulkarni A, et al. Highly sensitive and selective gas sensor using hydrophilic and hydrophobic graphenes. Sci Rep. 2013;3:1868.
[123] Duy LT, Kim DJ, Trung TQ, Dang VQ, Kim BY, Moon HK, et al. High performance three-dimensional chemical sensor platform using reduced graphene oxide formed on high aspect-ratio micro-pillars. Adv Funct Mater. 2015;25(6):883–90.
[124] Veluswamy P, Sathiyamoorthy S, Santhoshkumar P, Karunakaran G, Lee CW, Kuznetsov D, Kadarkaraithangam J, et al. Sono-synthesis approach of reduced graphene oxide for ammonia vapour detection at room temperature. Ultrason Sonochem. 2018;48:555–66.
[125] Mao S, Cui S, Lu G, Yu K, Wen Z, Chen J. Tuning gas-sensing properties of reduced graphene oxide using tin oxide nanocrystals. J Mater Chem. 2012;22(22):11009–13.
[126] Panda D, Nandi A, Datta SK, Saha H, Majumdar S. Selective detection of carbon monoxide (CO) gas by reduced graphene

oxide (rGO) at room temperature. RSC Adv. 2016;6(53):47337–48.
[127] Lee K, Yoo YK, Chae MS, Hwang KS, Lee J, Kim H, et al. Highly selective reduced graphene oxide (rGO) sensor based on a peptide aptamer receptor for detecting explosives. Sci Rep. 2019;9(1):1–9.
[128] Zhang LS, Wang WD, Liang XQ, Chu WS, Song WG, Wang W, et al. Characterization of partially reduced graphene oxide as room temperature sensor for H_2. Nanoscale. 2011;3(6):2458–60.
[129] Lipatov A, Varezhnikov A, Wilson P, Sysoev V, Kolmakov A, Sinitskii A. Highly selective gas sensor arrays based on thermally reduced graphene oxide. Nanoscale. 2013;5(12):5426–34.
[130] Robinson JT, Perkins FK, Snow ES, Wei Z, Sheehan PE. Reduced graphene oxide molecular sensors. Nano Lett. 2008;8(10):3137–40.
[131] Li X, Zhou X, Guo H, Wang C, Liu J, Sun P, et al. Design of Au@ ZnO yolk–shell nanospheres with enhanced gas sensing properties. ACS Appl Mater Interfaces. 2014;6(21):18661–7.
[132] Wang L, Lou Z, Deng J, Zhang R, Zhang T. Ethanol gas detection using a yolk–shell (core–shell) α-Fe_2O_3 nanospheres as sensing material. ACS Appl Mater Interfaces. 2015;7(23):13098–104.
[133] Yang X, Zhang S, Zhao L, Sun P, Wang T, Liu F, et al. One step synthesis of branched SnO_2/ZnO heterostructures and their enhanced gas-sensing properties. Sens Actuators B Chem. 2019;281:415–23.
[134] Ma ZH, Yu RT, Song JM. Facile synthesis of Pr-doped In_2O_3 nanoparticles and their high gas sensing performance for ethanol. Sens Actuators B Chem. 2020;305:127377.
[135] Hu L, Hu P, Chen Y, Lin Z, Qiu C. Synthesis and gas-sensing property of highly self-assembled tungsten oxide nanosheets. Front Chem. 2018;6:452.
[136] Sui L, Yu T, Zhao D, Cheng X, Zhang X, Wang P, et al. *In situ* deposited hierarchical CuO/NiO nanowall arrays film sensor with enhanced gas sensing performance to H_2S. J Hazard Mater. 2020;385:121570.
[137] Feng C, Kou X, Chen B, Qian G, Sun Y, Lu G. One-pot synthesis of In doped NiO nanofibers and their gas sensing properties. Sens Actuators B Chem. 2017;253:584–91.
[138] Wang T, Liu B, Li Q, Wang S. Controllable construction of Cr_2O_3–ZnO hierarchical heterostructures and their formaldehyde gas sensing properties. Mater Lett. 2018;221:260–3.
[139] Cao J, Wang S, Zhang H, Zhang T. Facile construction of Co_3O_4 porous microspheres with enhanced acetone gas sensing performances. Mater Sci Semicond Process. 2019;101:10–5.
[140] Kim HJ, Lee JH. Highly sensitive and selective gas sensors using p-type oxide semiconductors: overview. Sens Actuators B Chem. 2014;192:607–27.
[141] Latif U, Dickert FL. Graphene hybrid materials in gas sensing applications. Sensors. 2015;15(12):30504–24.
[142] Yi J, Lee JM, Park WI. Vertically aligned ZnO nanorods and graphene hybrid architectures for high-sensitive flexible gas sensors. Sens Actuators B Chem. 2011;155(1):264–9.
[143] Singh G, Choudhary A, Haranath D, Joshi AG, Singh N, Singh S, et al. ZnO decorated luminescent graphene as a potential gas sensor at room temperature. Carbon. 2012;50(2):385–94.
[144] Cuong TV, Pham VH, Chung JS, Shin EW, Yoo DH, Hahn SH, et al. Solution-processed ZnO-chemically converted graphene gas sensor. Mater Lett. 2010;64(22):2479–82.
[145] Deng S, Tjoa V, Fan HM, Tan HR, Sayle DC, Olivo M, et al. Reduced graphene oxide conjugated Cu_2O nanowire mesocrystals for high-performance NO_2 gas sensor. J Am Chem Soc. 2012;134(10):4905–17.
[146] Yamaura H, Moriya K, Miura N, Yamazoe N. Mechanism of sensitivity promotion in CO sensor using indium oxide and cobalt oxide. Sens Actuators B Chem. 2000;65(1–3):39–41. Sens Actuators B Chem. 2001;77(1–2):330–334.
[147] Choi US, Sakai G, Shimanoe K, Yamazoe N. Sensing properties of SnO_2–Co_3O_4 composites to CO and H_2. Sens Actuators B Chem. 2004;98(2–3):166–73.
[148] Cao AM, Hu JS, Liang HP, Song WG, Wan LJ, He XL, et al. Hierarchically structured cobalt oxide (Co_3O_4): the morphology control and its potential in sensors. J Phys Chem B. 2006;110(32):15858–63.
[149] Chen N, Li X, Wang X, Yu J, Wang J, Tang Z, et al. Enhanced room temperature sensing of Co_3O_4-intercalated reduced graphene oxide based gas sensors. Sens Actuators B Chem. 2013;188:902–8.
[150] Seo MH, Yuasa M, Kida T, Huh JS, Shimanoe K, Yamazoe N. Gas sensing characteristics and porosity control of nanostructured films composed of TiO_2 nanotubes. Sens Actuators B Chem. 2009;137(2):513–20.
[151] Liang Y, Li Y, Wang H, Zhou J, Wang J, Regier T, et al. Co_3O_4 nanocrystals on graphene as a synergistic catalyst for oxygen reduction reaction. Nat Mater. 2011;10(10):780–6.
[152] Zhang B, Cheng M, Liu G, Gao Y, Zhao L, Li S, et al. Room temperature NO_2 gas sensor based on porous Co_3O_4 slices/reduced graphene oxide hybrid. Sens Actuators B Chem. 2018;263:387–99.
[153] Pan J, Liu W, Quan L, Han N, Bai S, Luo R, et al. Cu_2O and rGO hybridizing for enhancement of low-concentration NO_2 sensing at room temperature. Ind Eng Chem Res. 2018;57(31):10086–94.
[154] Lassesson A, Schulze M, Van Lith J, Brown SA. Tin oxide nanocluster hydrogen and ammonia sensors. Nanotechnology. 2007;19(1):015502.
[155] Chen Z, Pan D, Zhao B, Ding G, Jiao Z, Wu M, et al. Insight on fractal assessment strategies for tin dioxide thin films. ACS Nano. 2010;4(2):1202–8.
[156] Gyger F, Hübner M, Feldmann C, Barsan N, Weimar U. Nanoscale SnO_2 hollow spheres and their application as a gas-sensing material. Chem Mater. 2010;22(16):4821–7.
[157] Fan G, Wang Y, Hu M, Luo Z, Li G. Synthesis of flowerlike nano-SnO_2 and a study of its gas sensing response. Meas Sci Technol. 2011;22(4):045203.
[158] Gurlo A. Nanosensors: towards morphological contol of gas sensing activity. SnO_2, In_2O_3, ZnO and WO_3 case studies. Nanoscale. 2011;3(1):154–65.
[159] Neri G, Leonardi SG, Latino M, Donato N, Baek S, Conte DE, et al. Sensing behavior of SnO_2/reduced graphene oxide nanocomposites toward NO_2. Sens Actuators B Chem. 2013;179:61–8.
[160] Zhang H, Feng J, Fei T, Liu S, Zhang T. SnO_2 nanoparticles-reduced graphene oxide nanocomposites for NO_2 sensing at low operating temperature. Sens Actuators B Chem. 2014;190:472–8.
[161] Cui S, Wen Z, Mattson EC, Mao S, Chang J, Weinert M, et al. Indium-doped SnO_2 nanoparticle–graphene nanohybrids:

simple one-pot synthesis and their selective detection of NO_2. J Mater Chem A. 2013;1(14):4462–7.
[162] Su J, Guo L, Bao N, Grimes CA. Nanostructured $WO_3/BiVO_4$ heterojunction films for efficient photoelectrochemical water splitting. Nano Lett. 2011;11(5):1928–33.
[163] Rossinyol E, Prim A, Pellicer E, Arbiol J, Hernández-Ramírez F, Peiro F, et al. Synthesis and characterization of chromium-doped mesoporous tungsten oxide for gas sensing applications. Adv Funct Mater. 2007;17(11):1801–6.
[164] Hung CM, Van Duy N, Van Quang V, Van Toan N, Van Hieu N, Hoa ND. Facile synthesis of ultrafine rGO/WO_3 nanowire nanocomposites for highly sensitive toxic NH_3 gas sensors. Mater Res Bull. 2020;125:110810.
[165] Jiang Z, Chen W, Jin L, Cui F, Song Z, Zhu C. High performance acetylene sensor with heterostructure based on WO_3 nanolamellae/reduced graphene oxide (rGO) nanosheets operating at low temperature. Nanomater. 2018;8(11):909.
[166] Su PG, Peng SL. Fabrication and NO_2 gas-sensing properties of reduced graphene oxide/WO_3 nanocomposite films. Talanta. 2015;132:398–405.
[167] Punetha D, Pandey SK. Sensitivity enhancement of ammonia gas sensor based on hydrothermally synthesized rGO/WO_3 nanocomposites. IEEE Sens J. 2019;20(4):1738–45.
[168] He JQ, Yin J, Liu D, Zhang LX, Cai FS, Bie LJ. Enhanced acetone gas-sensing performance of La_2O_3-doped flowerlike ZnO structure composed of nanorods. Sens Actuators B Chem. 2013;182:170–5.
[169] Na CW, Park SY, Lee JH. Punched ZnO nanobelt networks for highly sensitive gas sensors. Sens Actuators B Chem. 2012;174:495–9.
[170] Das S, Roy S, Bhattacharya TS, Sarkar CK. Efficient room temperature hydrogen gas sensor using ZnO nanoparticles-reduced graphene oxide nanohybrid. IEEE Sens J. 2020;21(2):1264–72.
[171] Liu J, Li S, Zhang B, Xiao Y, Gao Y, Yang Q, et al. Ultrasensitive and low detection limit of nitrogen dioxide gas sensor based on flower-like ZnO hierarchical nanostructure modified by reduced graphene oxide. Sens Actuators B Chem. 2017;249:715–24.
[172] Cao P, Cai Y, Pawar D, Navale ST, Rao CN, Han S, et al. Down to ppb level NO_2 detection by ZnO/rGO heterojunction based chemiresistive sensors. Chem Eng J. 2020;401:125491.
[173] Tang Z, Deng X, Zhang Y, Guo X, Yang J, Zhu C, et al. MoO_3 nanoflakes coupled reduced graphene oxide with enhanced ethanol sensing performance and mechanism. Sens Actuators B Chem. 2019;297:126730.
[174] Bai S, Chen C, Luo R, Chen A, Li D. Synthesis of MoO_3/reduced graphene oxide hybrids and mechanism of enhancing H_2S sensing performances. Sens Actuators B Chem. 2015;216:113–20.
[175] Ye Z, Tai H, Xie T, Yuan Z, Liu C, Jiang Y. Room temperature formaldehyde sensor with enhanced performance based on reduced graphene oxide/titanium dioxide. Sens Actuators B Chem. 2016;223:149–56.
[176] Li X, Zhao Y, Wang X, Wang J, Gaskov AM, Akbar SA. Reduced graphene oxide (rGO) decorated TiO_2 microspheres for selective room-temperature gas sensors. Sens Actuators B Chem. 2016;230:330–6.
[177] Ye Z, Tai H, Guo R, Yuan Z, Liu C, Su Y, et al. Excellent ammonia sensing performance of gas sensor based on graphene/titanium dioxide hybrid with improved morphology. Appl Surf Sci. 2017;419:84–90.
[178] Sadasivuni KK, Ponnamma D, Kim J, Thomas S. Graphene-based polymer nanocomposites in electronics. Germany: Springer; 2015.
[179] Kasap S, Capper P. Molecular electronics. In Springer handbook of electronic and photonic materials. Germany: Springer; 2017. p. 1257–79.
[180] Khan AA, Khan A, Rahman MM, Asiri AM, Oves M. Sensor development of 1, 2 dichlorobenzene based on polypyrole/Cu-doped ZnO (PPY/CZO) nanocomposite embedded silver electrode and their antimicrobial studies. Int J Biol Macromol. 2017;98:256–67.
[181] Rahman MM, Hussein MA, Alamry KA, Al-Shehry FM, Asiri AM. Polyaniline/graphene/carbon nanotubes nanocomposites for sensing environmentally hazardous 4-aminophenol. Nano-Struct Nano-Objects. 2018;15:63–74.
[182] Husain A, Ahmad S, Mohammad F. Synthesis, characterisation and ethanol sensing application of polythiophene/graphene nanocomposite. Mater Chem Phys. 2020;239:122324.
[183] Beduk T, Bihar E, Surya SG, Castillo AN, Inal S, Salama KN. A paper-based inkjet-printed PEDOT: PSS/ZnO sol–gel hydrazine sensor. Sens Actuators B Chem. 2020;306:127539.
[184] Shah AH. Applications of carbon nanotubes and their polymer nanocomposites for gas sensors. In Carbon nanotubes-current progress of their polymer composites. IntechOpen; 2016;459–94.
[185] Mora A, Han F, Lubineau GL. Estimating and understanding the efficiency of nanoparticles in enhancing the conductivity of carbon nanotube/polymer composites. Results Phys. 2018;10:81–90.
[186] Andre RS, Shimizu FM, Miyazaki CM, Riul Jr A, Manzani D, Ribeiro SJ, et al. Hybrid layer-by-layer (LbL) films of polyaniline, graphene oxide and zinc oxide to detect ammonia. Sens Actuators B Chem. 2017;238:795–801.
[187] Huang X, Hu N, Gao R, Yu Y, Wang Y, Yang Z, et al. Reduced graphene oxide–polyaniline hybrid: preparation, characterization and its applications for ammonia gas sensing. J Mater Chem. 2012;22(42):22488–95.
[188] Li S, Wang T, Yang Z, He J, Wang J, Zhao L, et al. Room temperature high performance NH_3 sensor based on GO-rambutan-like polyaniline hollow nanosphere hybrid assembled to flexible PET substrate. Sens Actuators B Chem. 2018;273:726–34.
[189] Zhang D, Wu Z, Zong X. Flexible and highly sensitive H_2S gas sensor based on in situ polymerized SnO_2/rGO/PANI ternary nanocomposite with application in halitosis diagnosis. Sens Actuators B Chem. 2019;289:32–41.
[190] Xie T, Xie G, Zhou Y, Huang J, Wu M, Jiang Y, et al. Thin film transistors gas sensors based on reduced graphene oxide poly (3-hexylthiophene) bilayer film for nitrogen dioxide detection. Chem Phys Lett. 2014;614:275–81.
[191] Ye Z, Jiang Y, Tai H, Yuan Z. The investigation of reduced graphene oxide/P_3HT composite films for ammonia detection. Integr Ferroelectr. 2014;154(1):73–81.
[192] Yang Y, Yang X, Yang W, Li S, Xu J, Jiang Y. Porous conducting polymer and reduced graphene oxide nanocomposites for room temperature gas detection. RSC Adv. 2014;4(80):42546–53.

[193] Pasha A, Khasim S, Khan FA, Dhananjaya N. Fabrication of gas sensor device using poly (3, 4-ethylenedioxythiophene)-poly (styrenesulfonate)-doped reduced graphene oxide organic thin films for detection of ammonia gas at room temperature. Iran Polym J. 2019;28(3):183–92.
[194] Qin Y, Zhang B, Zhang Z. Combination of PPy with three-dimensional rGO to construct bioinspired nanocomposite for NH_3-sensing enhancement. Org Electron. 2019;70:240–5.
[195] Yu X, Zhang W, Zhang P, Su Z. Fabrication technologies and sensing applications of graphene-based composite films: advances and challenges. Biosens Bioelectron. 2017;89:72–84.
[196] Zhou L, Shen F, Tian X, Wang D, Zhang T, Chen W. Stable Cu_2O nanocrystals grown on functionalized graphene sheets and room temperature H_2S gas sensing with ultrahigh sensitivity. Nanoscale. 2013;5(4):1564–9.
[197] Hong J, Lee S, Seo J, Pyo S, Kim J, Lee T. A highly sensitive hydrogen sensor with gas selectivity using a PMMA membrane-coated Pd nanoparticle/single-layer graphene hybrid. ACS Appl Mater Interfaces. 2015;7(6):3554–61.
[198] Al-Mashat L, Shin K, Kalantar-Zadeh K, Plessis JD, Han SH, Kojima RW, et al. Graphene/polyaniline nanocomposite for hydrogen sensing. J Phys Chem C. 2010;114(39):16168–73.
[199] Parmar M, Balamurugan C, Lee DW. PANI and graphene/PANI nanocomposite films – Comparative toluene gas sensing behavior. Sensors. 2013;13(12):16611–24.
[200] Xiang C, Jiang D, Zou Y, Chu H, Qiu S, Zhang H, et al. Ammonia sensor based on polypyrrole–graphene nanocomposite decorated with titania nanoparticles. Ceram Int. 2015;41(5):6432–8.
[201] Seekaew Y, Lokavee S, Phokharatkul D, Wisitsoraat A, Kerdcharoen T, Wongchoosuk C. Low-cost and flexible printed graphene–PEDOT: PSS gas sensor for ammonia detection. Org Electron. 2014;15(11):2971–81.
[202] Dehsari HS, Gavgani JN, Hasani A, Mahyari M, Shalamzari EK, Salehi A, et al. Copper(II) phthalocyanine supported on a three-dimensional nitrogen-doped graphene/PEDOT-PSS nanocomposite as a highly selective and sensitive sensor for ammonia detection at room temperature. RSC Adv. 2015;5(97):79729–37.
[203] Gavgani JN, Hasani A, Nouri M, Mahyari M, Salehi A. Highly sensitive and flexible ammonia sensor based on S and N co-doped graphene quantum dots/polyaniline hybrid at room temperature. Sens Actuators B Chem. 2016;229:239–48.
[204] Hakimi M, Salehi A, Boroumand FA, Mosleh N. Fabrication of a room temperature ammonia gas sensor based on polyaniline with N-doped graphene quantum dots. IEEE Sens J. 2018;18(6):2245–52.
[205] An X, Jimmy CY, Wang Y, Hu Y, Yu X, Zhang G. WO_3 nanorods/graphene nanocomposites for high-efficiency visible-light-driven photocatalysis and NO_2 gas sensing. J Mater Chem. 2012;22(17):8525–31.
[206] Esfandiar A, Irajizad A, Akhavan O, Ghasemi S, Gholami MR. Pd–WO_3/reduced graphene oxide hierarchical nanostructures as efficient hydrogen gas sensors. Int J Hydrog Energy. 2014;39(15):8169–79.
[207] Wu Z, Chen X, Zhu S, Zhou Z, Yao Y, Quan W, et al. Enhanced sensitivity of ammonia sensor using graphene/polyaniline nanocomposite. Sens Actuators B Chem. 2013;178:485–93.
[208] Tian J, Yang G, Jiang D, Su F, Zhang Z. A hybrid material consisting of bulk-reduced TiO_2, graphene oxide and polyaniline for resistance based sensing of gaseous ammonia at room temperature. Microchim Acta. 2016;183(11):2871–8.
[209] Lu G, Ocola LE, Chen J. Gas detection using low-temperature reduced graphene oxide sheets. Appl Phys Lett. 2009;94(8):083111.
[210] Fowler JD, Allen MJ, Tung VC, Yang Y, Kaner RB, Weiller BH. Practical chemical sensors from chemically derived graphene. ACS Nano. 2009;3(2):301–6.
[211] Liu X, Cui J, Sun J, Zhang X. 3D graphene aerogel-supported SnO_2 nanoparticles for efficient detection of NO_2. RSC Adv. 2014;4(43):22601–5.
[212] Xiao Y, Yang Q, Wang Z, Zhang R, Gao Y, Sun P, et al. Improvement of NO_2 gas sensing performance based on discoid tin oxide modified by reduced graphene oxide. Sens Actuators B. 2016;227:419–26.
[213] Srivastava S, Jain K, Singh VN, Singh S, Vijayan N, Dilawar N, et al. Faster response of NO_2 sensing in graphene–WO_3 nanocomposites. Nanotechnology. 2012;23(20):205501.
[214] Jie X, Zeng D, Zhang J, Xu K, Wu J, Zhu B, et al. Graphene-wrapped WO_3 nanospheres with room-temperature NO_2 sensing induced by interface charge transfer. Sens Actuators B Chem. 2015;220:201–9.
[215] Liu X, Li J, Sun J, Zhang X. 3D Fe_3O_4 nanoparticle/graphene aerogel for NO_2 sensing at room temperature. RSC Adv. 2015;5(90):73699–704.
[216] Liu X, Sun J, Zhang X. Novel 3D graphene aerogel–ZnO composites as efficient detection for NO_2 at room temperature. Sens Actuators B Chem. 2015;211:220–6.
[217] Abideen ZU, Katoch A, Kim JH, Kwon YJ, Kim HW, Kim SS. Excellent gas detection of ZnO nanofibers by loading with reduced graphene oxide nanosheets. Sens Actuators B Chem. 2015;221:1499–507.
[218] Huang XL, Hu NT, Wang YY, Zhang YF. Ammonia gas sensor based on aniline reduced graphene oxide. In Advanced materials research. Trans Tech Publications Ltd; 2013;669:79–84.
[219] Bai S, Zhao Y, Sun J, Tian Y, Luo R, Li D, et al. Ultrasensitive room temperature NH_3 sensor based on a graphene–polyaniline hybrid loaded on PET thin film. Chem Comm. 2015;51(35):7524–7.
[220] Ye Z, Jiang Y, Tai H, Guo N, Xie G, Yuan Z. The investigation of reduced graphene oxide@ SnO_2–polyaniline composite thin films for ammonia detection at room temperature. J Mater Sci Mater Electron. 2015;26(2):833–41.
[221] Lin Q, Li Y, Yang M. Tin oxide/graphene composite fabricated *via* a hydrothermal method for gas sensors working at room temperature. Sens Actuators B Chem. 2012;173:139–47.
[222] Zhou Y, Jiang Y, Xie G, Wu M, Tai H. Gas sensors for CO_2 detection based on RGO–PEI films at room temperature. Chin Sci Bull. 2014;59(17):1999–2005.
[223] Naikoo RA, Tomar R. Fabrication of a novel Zeolite-X/Reduced graphene oxide/Polypyrrole nanocomposite and its role in sensitive detection of CO. Mater Chem Phys. 2018;211:225–33.
[224] Mishra SK, Tripathi SN, Choudhary V, Gupta BD. Surface plasmon resonance-based fiber optic methane gas sensor utilizing graphene-carbon nanotubes-poly(methyl methacrylate) hybrid nanocomposite. Plasmonics. 2015;10(5):1147–57.